science.sciencemag.org/content/371/6524/52/suppl/DC1

Supplementary Materials for

Airway stem cells sense hypoxia and differentiate into protective solitary neuroendocrine cells

Manjunatha Shivaraju, Udbhav K. Chitta, Robert M. H. Grange, Isha H. Jain, Diane Capen, Lan Liao, Jianming Xu, Fumito Ichinose, Warren M. Zapol, Vamsi K. Mootha, Jayaraj Rajagopal*

*Corresponding author. Email: jrajagopal@partners.org

Published 1 January 2021, *Science* **371**, 52 (2021)
DOI: 10.1126/science.aba0629

This PDF file includes:

Other Supplementary Materials for this manuscript include the following:
(available at science.sciencemag.org/content/371/6524/52/suppl/DC1)

MDAR Reproducibility Checklist

Materials and Methods

Animals

Mouse models *Ascl1-CreER* (*36*), *p63-CreER* (*37*), and *Scgb1a1-CreER* (*38*), and *Cgrp-CreER* (*14*) mice were previously described. *Hif1a*$^{fl/fl}$ (stock number 007561), *Hif2a*$^{fl/fl}$ (stock number 008407), Phd1, Phd2, Phd3 triple floxed (stock number 028097)**,** C57BL/6J (stock no. 000664), LSL-tdTomato (stock no. 007914), and ROSA-DTA (stock no. 009669), were purchased from The Jackson Laboratory (Bar Harbor, ME). *Cgrp-CreER* (a gift from Pao-Tien Chuang) females were crossed to LSL-tdTomato mice to obtain double transgenic mice. *Cgrp-CreER* and floxed DTA mice used were heterozygous. To label cells, we injected tamoxifen intraperitoneally (2mg/20gms body weight) for three consecutive days to induce the Cre-mediated excision of a stop codon and subsequent expression of tdTomato. Both male and female 8-12-week old mice were used for experiments. Control and treated animals were age matched. We analyzed at least 4-8 mice per condition in each experiment. The MGH Subcommittee on Research Animal Care approved animal protocols in accordance with NIH guidelines.

Tissue harvest, sectioning, and staining

Mice were euthanized with carbon dioxide gas. All the tissues were harvested and fixed at 4℃ for 1 hour and 30 minutes or overnight with fresh 4% paraformaldehyde (PFA). The tissues were then rinsed with PBS 4 times (5 min each) and incubated in 30% sucrose in PBS at 4oC overnight. Afterwards, the tissues are soaked in Tissue-Tek® O.C.T. Compound for 1 hour and then frozen in O.C.T. for cryosectioning at 7 μm thickness. Cryosections (7 μm) were permeabilized with 0.1% Triton X-100 in PBS, blocked in 1% BSA for 10 minutes at room temperature, incubated with primary antibodies for 1 hour at room temperature or overnight at 4℃, washed, incubated with

appropriate secondary antibodies diluted in blocking buffer for 45 minutes at room temperature, washed, and counterstained with DAPI.

The following primary antibodies were used: mouse anti- chromogranin A (1:200; SC-393941, Santacruz), rabbit anti - PGP9.5 (1:200, AS-53772, Anaspec), rabbit anti-Ki67 (1:200; ab15580, Abcam); rat anti-Ki67 (1:200; 14-5698-82, eBioscience); rabbit anti-cleaved caspase-3 (1:100; CST-9661S); goat anti-SCGB1A1 (1:500; kindly provided by Barry Stripp); rabbit anti-p63 (1:200; GTX102425, GeneTex); mouse anti-tubulin, acetylated (1:100; T6793, Sigma); mouse anti-BrdU (1:200; Thermo Fisher (B35128); anti-HIF-1α (Novus Biologicals, NB100-134, 1: 3000), anti-HIF-2α (Novus Biologicals, NB100-122, 1:2000), anti-tubulin (Novus Biologicals, NB600-936, 1:5000), anti-RAMP1 (Abcam, ab203282, 1:100), anti-CRLR (Abcam, ab83697, 1:100). Neuroendocrine master mix for the human samples (chromogranin A + Synaptophysin); mouse anti-Synaptophysin Bond RTU Primary (1:50; PA0299, Leica Biosystems), mouse chromogranin 5H7 Bond RTU (1:50; PA0515, Leica Biosystems). Promega DeadEnd^{TM} Fluorometric TUNEL System (G3250, Thermo Fisher Scientific) used to detect cell death.

All secondary antibodies were Alexa Fluor conjugates (488, 594 and 647) and used at 1:400 dilution (Life Technologies). Images were obtained using Olympus Fluoview FV10i Confocal Microscope (Olympus, Center Valley, PA). Cells were manually counted based on immunofluorescence staining of markers for each of the respective cell types. Cartilage 1 to 10 was used as reference points in all the tracheal whole mount or cross section samples to count specific cell types based on immunostaining. Serial sections were stained for the antibodies tested and randomly selected slides were used for cell counting. For whole mount fluorescence of tissues, trachea was dissected in ice-cold PBS and washed 3 times in PBS then mounted on a slide. Images

were obtained using Olympus Fluoview FV10i Confocal Microscope (Olympus, Center Valley, PA).

Administration of FG-4592, cobalt chloride, CGRP, BIBN-4096, 4- hydroxytamoxifen, and Bromodeoxyuridine / 5-bromo-2'-deoxyuridine (BrdU).

FG-4592 was dissolved in 5% dextrose and administered as 10 doses (100mg/Kg) over 20 days (48hr intervals) intraperitoneally. For intranasal administration of small molecule or chemicals, mice were anesthetized with 4% isoflurane (sigma Aldrich) and 100% oxygen in an anesthetic chamber (with sliding cover, Evonik Plexiglas, 240 × 140 × 120 mm), which was not prefilled in order to prevent distress. Cobalt chloride was administered as 10 doses (70 µl of 20mM) over 20 days (24hr interval) intranasally. 30 µl of αCGRP (0.1nM) and BIBN-4096 (10nM) were administered intranasally at the indicated concentrations and intervals. 4- hydroxytamoxifen (2µM) was administered as two drops, 30 µl each. Mice were monitored until they exhibited normal activity and were then returned to their respective cages. No lethality occurred during or after the administration procedure. BrdU (1mg/ml) was administered through drinking water for indicated period.

Hypoxia chamber experiments

Hypoxia exposures were done as described previously (*39*). Briefly, wildtype, *Ascl1*-CreER-tdTomato, *p63*-CreER-tdtomato, or *Scgb1a1*-CreER-tdTomato mice were exposed to hypoxia (8% O_2) or normoxia (21% O_2). Mice were placed in 60-liter plexiglass chambers containing a gas mixture of compressed air and 100% N_2 (Airgas Inc.). The gas flow rates were measured and controlled with rotameters and valves. Oxygen concentrations were measured several times each

day at the outlet of the chambers using an oxygen analyzer (MiniOx I Oxygen Analyzer, Ohio Medical Corporation) and the flow rates of air, nitrogen and oxygen were modified as necessary in order to obtain a stable oxygen concentration of 8% in the hypoxic chamber. Soda lime (Sodasorb, Smiths Medical) (approximately 250g), was placed on the floor of each chamber to scavenge carbon dioxide (CO_2) produced by the animals and replaced every 3 days. The CO_2 concentration in each chamber as well as the temperature and the humidity were monitored continuously using a dedicated infrared CO_2 analyzer, thermometer and humidity meter (Extech CO200 Monitor, Extech Instruments). The total flow of fresh gas flushing each chamber was adjusted between 5 and 10 L/min to maintain the chamber CO_2 level below 0.4% and the relative humidity between 30% and 70%. Mice were exposed to gas treatment continuously for 24 hours per day, 7 days a week. The chambers were briefly opened three times a week to evaluate the health status of the mice, clean the cages and add water and food.

For administration of 4-OH tamoxifen, CGRP, and/or BIBN4096, we removed the mice from the chambers, briefly anesthetized with 4% isoflurane (Sigma Aldrich) and 21% O_2 in an anesthetic chamber (with sliding cover, Evonik Plexiglas, 240 × 140 × 120 mm), which was not prefilled in order to prevent distress. Once the mice were inactive, we intranasally administered the 4-hydroxytamoxifen (total of 60 µl (2µM) in 2 drops) and/or CGRP (30 µl (0.1nM) and/or BIBN4096 (30 µl (10nM)). Once the mice were fully active, they were returned to their chambers. The entire administration procedure was completed in 30 min. No lethality occurred during or after the administration procedure.

Human airway stem cell isolation

Fresh discarded human tissue was obtained from New England Organ Bank. Bronchus segments were then dissected and cleared of connective tissues and blood cells. To dissociate airway epithelial cells, the bronchi are cut in several pieces and incubated at 4^{o}C without agitation for 1 day in DMEM/F12 medium containing 1 mg/ml pronase, 0.5 mg/ml DNase, 5 μM ROCK inhibitor Y-27632 and 1x Penicillin- Streptomycin (Pen/Strep). After that, the epithelial layer is scraped off gently using a cell scraper. The cell suspensions are filtered through 100 μm strainers and spun down. The cell pellets are rinsed 3 times with DMEM + 10% FBS. Epithelial basal cells were sorted by FACS with antibodies against EpCAM-PECy7 (1:50; 25-5791-80, eBiosciences) and GSIβ4 (Griffonia Simplicifolia Isolectin beta4)-Biotin (L2120, Sigma). BD FACS Aria (BD, San Jose, CA) and analysis was performed using FlowJo (version 10) software.

Mucociliary differentiation and NE differentiation on air-liquid interface

Human airway stem cell cultures were seeded onto 0.4 μm transwell membranes pre-coated with 804G-conditioned medium with a density of >6000 cells/mm2. After cell attachment for >12 hours, excess cells are removed and the medium is replaced with complete Pneumacult-ALI medium (StemCell Technology, Cat. 05001). The next day, ALI medium is added only in the lower chamber to initiate airway-liquid interface (*40*). Then the medium is changed daily until differentiation is well established. After 20 days of differentiation the ALI cultures were treated with FG-4592 (10μM in 0.1% DMSO) for 10 days to induce NE differentiation. To stain for neuroendocrine markers, the membranes are fixed with 4% PFA at room temperature for 10 min, followed by washing and permeabilization with PBS + 0.2% Triton X-100.

Electron microscopy

Intact tissue specimens were initially immersion-fixed in 2.5% glutaraldehyde in 0.1M sodium cacodylate buffer (pH 7.4, Electron Microscopy Sciences, Hatfield, PA) overnight at RT. Target tissue was excised and trimmed as needed and smaller pieces further fixed 24-48hrs in 2.5% glutaraldehyde in 0.1M sodium cacodylate buffer at 4°C. Specimens were rinsed several times in 0.1M sodium cacodylate buffer, post-fixed in 1.0% osmium tetroxide for 1hr at room temperature and rinsed again several times in cacodylate buffer. Samples were then dehydrated through an ethanol series to 100% ethanol and were then dehydrated briefly in 100% propylene oxide. Tissue was then allowed to pre-infiltrate 2hrs in a 2:1 mix of propylene oxide and Eponate resin (Ted Pella, Redding, CA), then transferred into a 1:1 mix of propylene oxide and Eponate resin and allowed to infiltrate overnight on a gentle rotator. The following day, specimens were transferred into a 2:1 mix of Eponate resin and propylene oxide for a minimum of 2 hrs, allowed to infiltrate on a gentle rotator in fresh 100% Eponate resin for several hours, and embedded (with specific attention to orientation) in fresh 100% Eponate in flat molds; polymerization occurred within 24-48 hrs at 60°C. Thin (70nm) sections were cut using a Leica EM UC7 ultramicrotome, collected onto formvar-coated grids, stained with uranyl acetate and Reynold's lead citrate and examined in a JEOL JEM 1011 transmission electron microscope at 80 kV. Images were collected using an AMT digital imaging system with proprietary image capture software (Advanced Microscopy Techniques, Danvers, MA).

Western blot analysis

Cells were lysed in lysis buffer (50 mM Tris/HCl, pH 7.5, 150 mM NaCl, 1% Triton X-100, 2 mM EDTA, 2 mM DTT) and complete proteinase inhibitors (Roche) for 20 min on ice and centrifuged at 12000rpm for 10min. Absorbance at 280 nm was used to quantify protein concentrations by Nanodrop 2000. Western blotting was performed according to standard protocol. Briefly, samples were run on NuPAGE 4%–12% Bis-Tris precast polyacrylamide gels (Thermofisher) and transferred onto the nitrocellulose membrane, blocked in 5% non-fat milk in TBST (Tris-buffered saline + 0.1% Tween-20). The following primary antibodies were used: anti-HIF-1α (Novus Biologicals, NB100-134, 1: 3000), anti-HIF-2α (Novus Biologicals, NB100-122, 1:2000) and Tubulin (Novus Biologicals, NB600-936, 1:5000), with the appropriate HRP-labeled secondary antibody and developed with ECL west pico plus (ThermoFisher Scientific). ImageJ was used to quantify the intensity of individual bands.

Statistical analysis: The standard error was calculated from the average of at least 3 independent tracheal/lung samples unless otherwise mentioned. Data was compared among groups using ANOVA analysis. A p-value of less than 0.05 was considered significant. The experimental data was analyzed without any pre-set bias and no particular criteria to exclude or include any specific sample from the analysis was used.

Fig. S1.

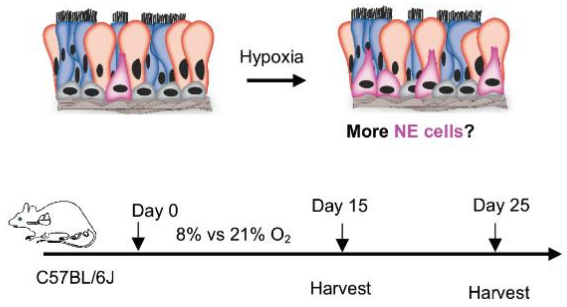

Fig. S1. (A) Schematic representation of hypoxia exposure protocol and assessment of NE cell numbers.

Fig. S2.

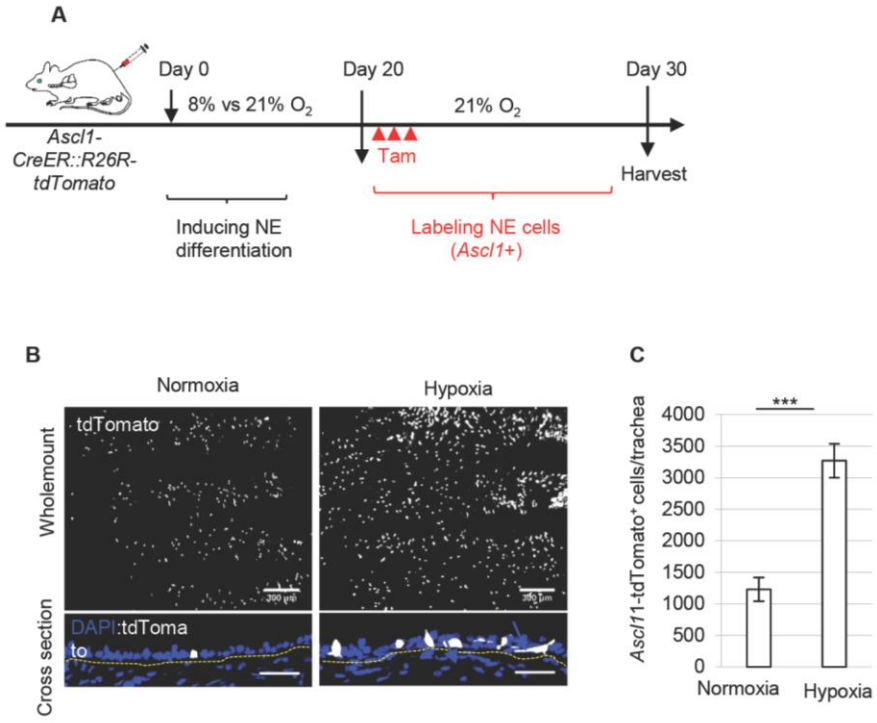

Fig. S2. Hypoxia leads to an increase in solitary neuroendocrine (NE) cell numbers in the adult mouse trachea measured by *Ascl1* driver line.

A) Schematic representation of induction of NE cell differentiation and subsequent labeling of *Ascl1*$^{+}$ solitary NE cells in *Ascl1-tdTomato* reporter mice. (B) Whole-mounts and cross sections of tracheal epithelium demonstrates a significant increase in the number of tdTomato+ cells in *Ascl1-tdTomato* reporter mice exposed to hypoxia for 20 days (n=4). Dotted lines indicate basement membrane. (C) Quantification of tdTomato^{+} solitary NE cells per trachea from *Ascl1-tdTomato* reporter mice subjected to hypoxia (n=4). *** p<0.001; Error bars, means ± standard deviation. Scale bars 20 μm unless indicated.

Fig. S3.

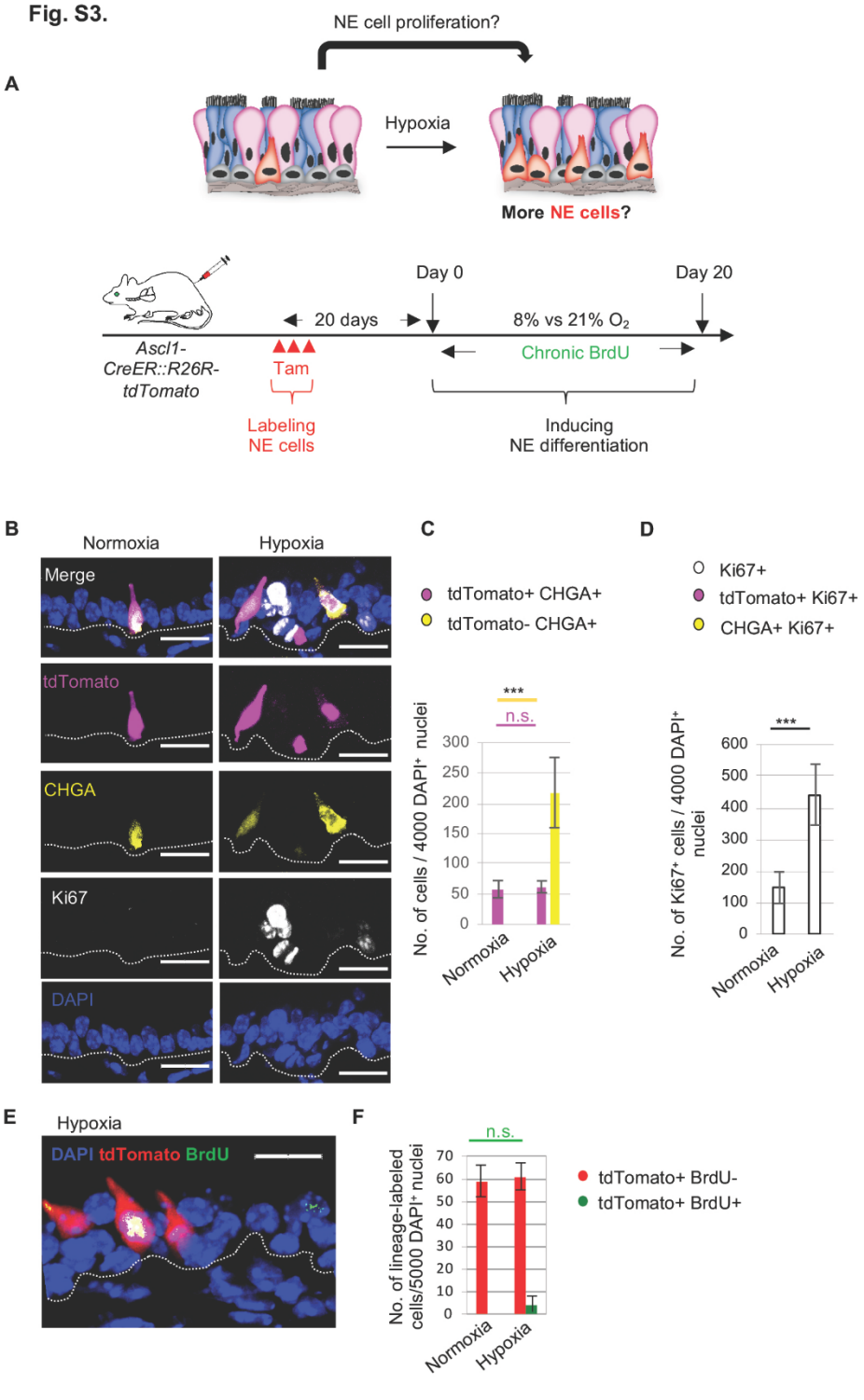
A
NE cell proliferation?
Hypoxia
More NE cells?
Day 0
Day 20
20 days
8% vs 21% O2
Chronic BrdU
Ascl1-CreER::R26R-tdTomato
Tam
Labeling NE cells
Inducing NE differentiation
B
Normoxia
Hypoxia
Merge
tdTomato
CHGA
Ki67
DAPI
C
tdTomato+ CHGA+
tdTomato- CHGA+
***
n.s.
No. of cells / 4000 DAPI+ nuclei
Normoxia
Hypoxia
D
Ki67+
tdTomato+ Ki67+
CHGA+ Ki67+
***
No. of Ki67+ cells / 4000 DAPI+ nuclei
Normoxia
Hypoxia
E
Hypoxia
DAPI tdTomato BrdU
F
n.s.
No. of lineage-labeled cells/5000 DAPI+ nuclei
tdTomato+ BrdU-
tdTomato+ BrdU+
Normoxia
Hypoxia

Fig. S3. Pre-existing NE cells do not expand following hypoxia.

(A) Schematic representation of lineage labeling of *Ascl1*$^{+}$ solitary NE cells in *Ascl1-tdTomato* reporter mice prior to the induction of hypoxia to lineage label pre-existing NE cells and administration of chronic BrdU. (B) Immunostaining for CHGA (yellow), and Ki67 (white), on tracheal sections from lineage-label *Ascl1-tdTomato* reporter mice that were exposed to hypoxia. Quantification of (C) tdTomato^{+} CHGA^{+} and tdTomato^{-} CHGA^{+} cells, (D) Ki67^{+}, tdTomato^{+} Ki67^{+}, and CHGA^{+} Ki67^{+} cells on tracheal sections from lineage-label *Ascl1-tdTomato* reporter mice that were exposed to hypoxia (n=5). (E) Immunostaining for BrdU (green) on tracheal sections from lineage-label *Ascl1-tdTomato* reporter mice that were exposed to hypoxia and quantification of (F) tdTomato^{+} BrdU^{+} and tdTomato^{+} BrdU^{-} cells. Dotted line indicates basement membrane. (n.s. = not significant. *** p <0.0001; error bars, means ± standard deviation. Scale bars 30 μm.

Fig. S4.

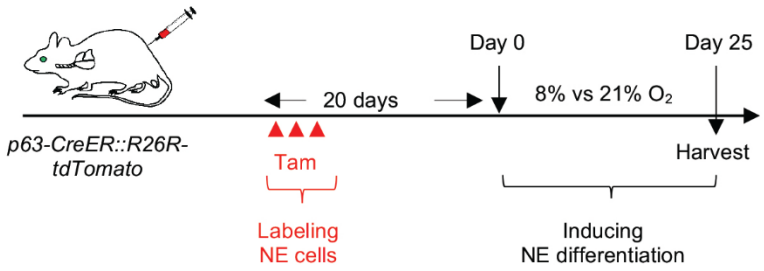

Fig. S4. Schematic representation of lineage labeling of $p63^{+}$ basal stem cells using *p63-tdTomato* reporter mice followed by induction of hypoxia to lineage label basal cells.

Fig. S5.

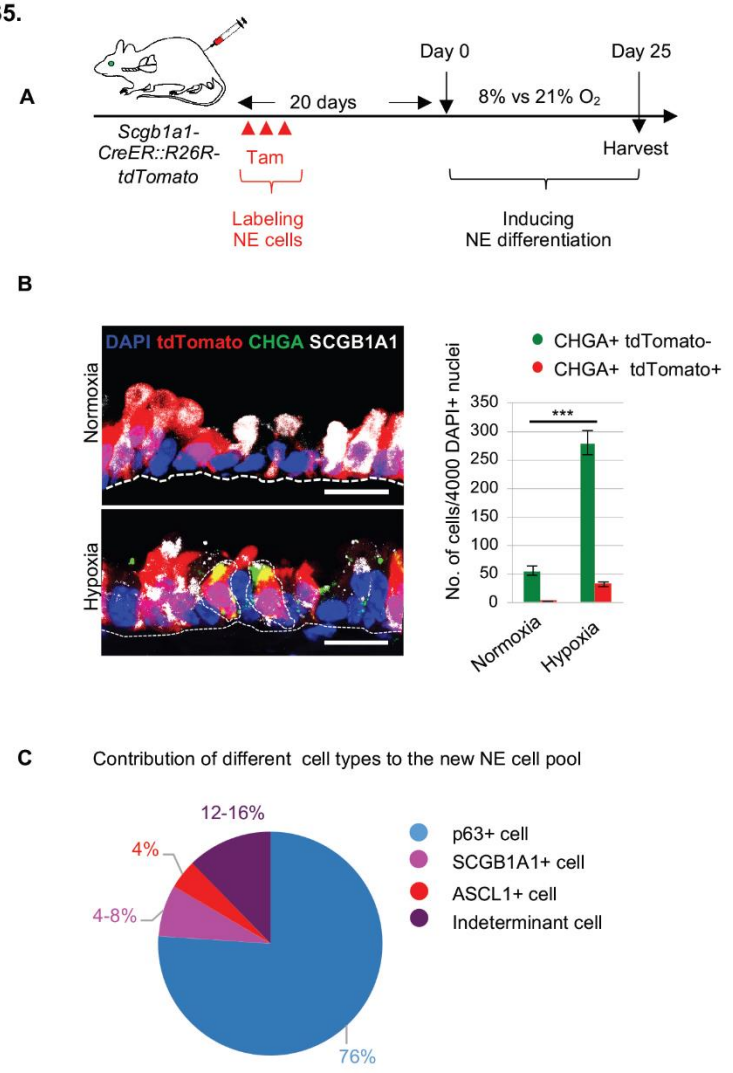

Fig. S5. Small number of secretory cells undergo NE differentiation

(A) Schematic representation of lineage labeling of secretory cells using *Scgb1a1-tdTomato* reporter mice followed by induction of hypoxia to lineage label secretory cells. (B) Immunostaining for the CHGA (green) and SCGB1A1 (white) on tracheal sections of *Scgb1a1-tdTomato* reporter mice and quantification of absolute numbers of $CHGA^{+}$ $tdTomato^{+}$ and $CHGA^{+}$ $tdTomato^{-}$ cells. (C) Contribution of different cell types to the new solitary NE cell pool. n.s.

indicates no significance, *** $p<0.001$ and * $p<0.05$; error bars, means ± standard deviation. Scale bars 20 μm unless indicated.

Fig. S6.

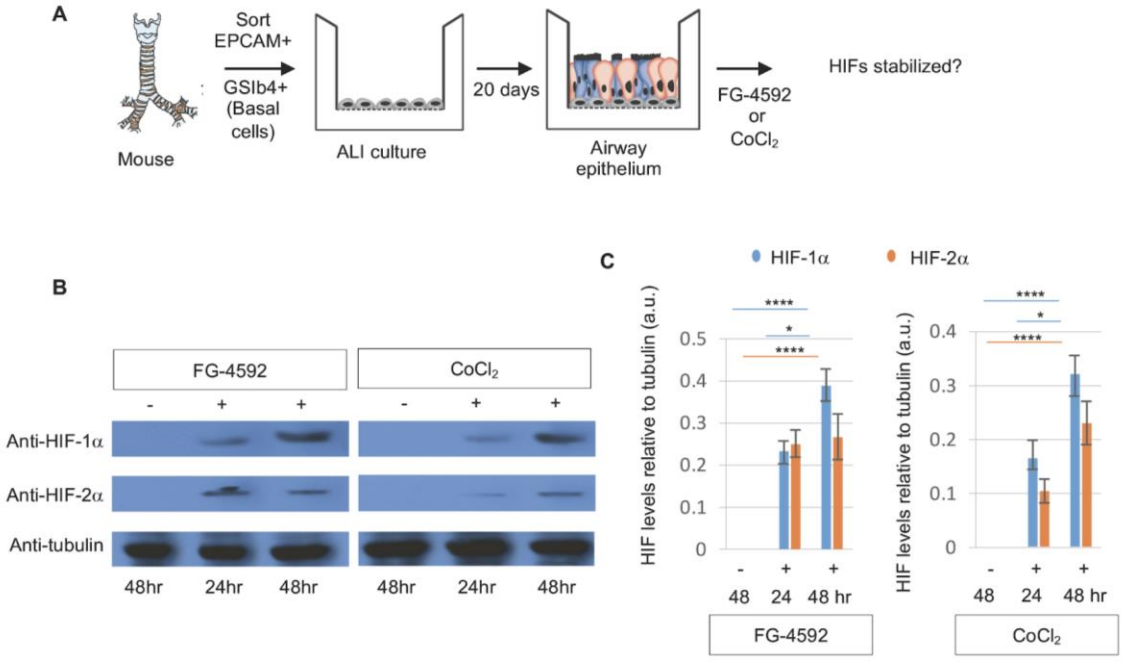

Fig. S6. FG-4592 and $CoCl_2$ administration stabilize HIF-1α and HIF-2α in ALI culture.

(A) Schematic representation of mouse tracheal basal stem cell isolation and treatment of airway epithelial cultures with FG-4592 and $CoCl_2$. (B) Western blot analysis of HIF-1α (120 kDa) (top row), HIF-2α (118 kDa) (middle row), and tubulin (50 kDa) (loading control) (bottom row) in whole epithelium differentiated using an ALI culture system. Left panel, ALI was treated with FG-4592, and right panel, ALI was treated with $CoCl_2$. (C) Quantification of HIF-1α and HIF-2α,

western blot signal from (B). ****p <0.0001 or * p <0.05; error bars, means ± standard deviation. a.u.= arbitrary units.

Fig. S7.

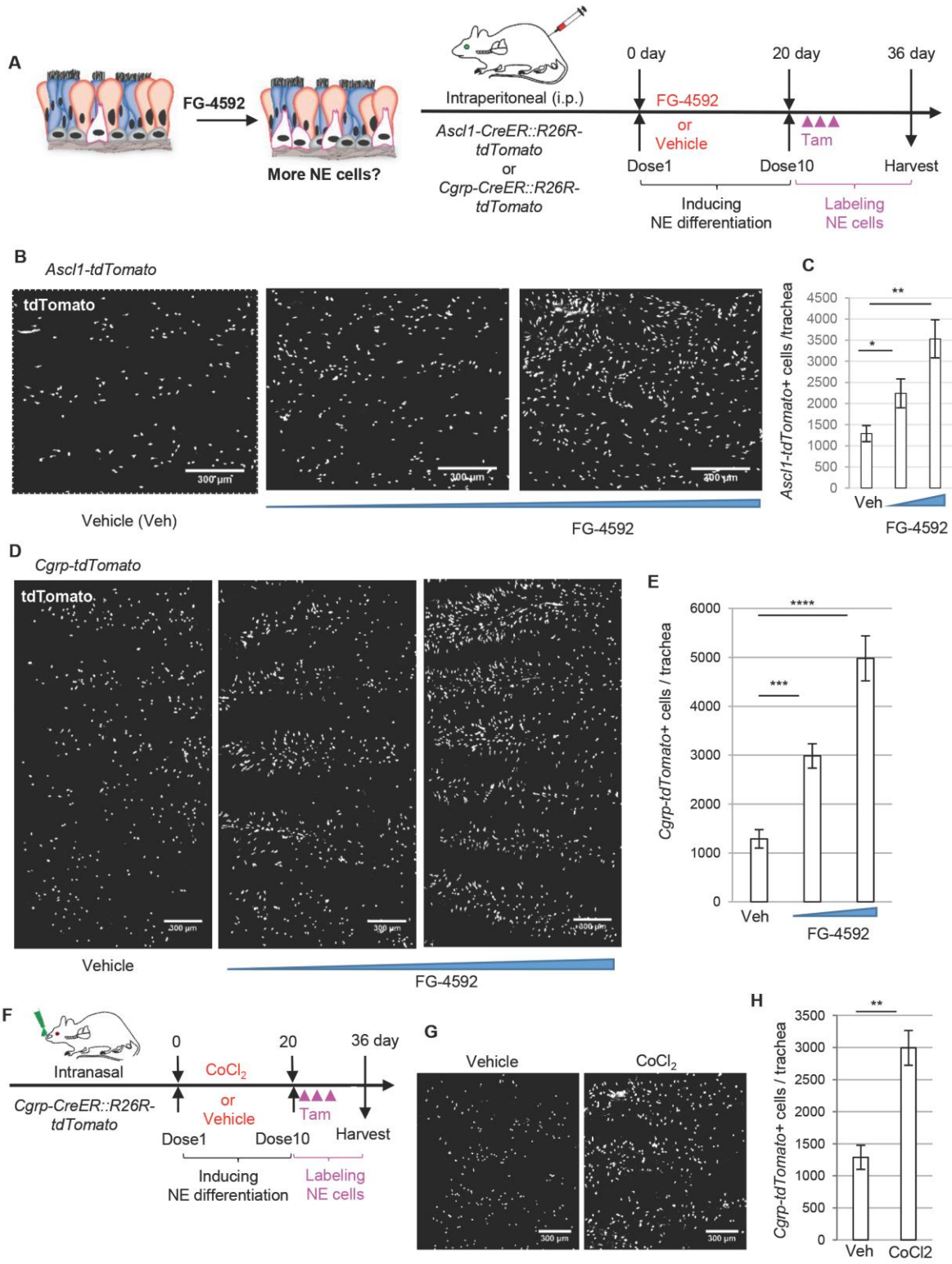
A
FG-4592
More NE cells?
Intraperitoneal (i.p.)
Ascl1-CreER::R26R-tdTomato
or
Cgrp-CreER::R26R-tdTomato
0 day
20 day
36 day
FG-4592
or
Vehicle
Tam
Dose1
Dose10
Harvest
Inducing NE differentiation
Labeling NE cells
B
Ascl1-tdTomato
tdTomato
300 μm
Vehicle (Veh)
FG-4592
C
Ascl1-tdTomato+ cells /trachea
4500
4000
3500
3000
2500
2000
1500
1000
500
0
**
*
Veh
FG-4592
D
Cgrp-tdTomato
tdTomato
300 μm
Vehicle
FG-4592
E
Cgrp-tdTomato+ cells / trachea
6000
5000
4000
3000
2000
1000
0
****
***
Veh
FG-4592
F
Intranasal
Cgrp-CreER::R26R-tdTomato
0
20
36 day
CoCl2
or
Vehicle
Tam
Dose1
Dose10
Harvest
Inducing NE differentiation
Labeling NE cells
G
Vehicle
CoCl2
300 μm
H
Cgrp-tdTomato+ cells / trachea
3500
3000
2500
2000
1500
1000
500
0
**
Veh
CoCl2

Fig. S7. Small molecule activation of the hypoxia response leads to an increase in solitary NE cells in the adult mouse trachea.

(A) Schematic representation of FG-4592 induction of NE differentiation and subsequent labeling of *Ascl1*$^{+}$ solitary NE cells using *Ascl1- tdTomato* reporter mice. (B) Whole-mount tracheal images showing a dose-dependent increase in the number of tdTomato^{+} solitary NE cells after intraperitoneal injection of FG-4592 in *Ascl1- tdTomato* reporter mice (n=8). (C) Quantification of tdTomato^{+} solitary NE cells per trachea from vehicle or FG4592-treated *Ascl1- tdTomato* mice (*n*=8). (D) Whole-mount tracheal images showing a dose-dependent increase in the number of tdTomato^{+} solitary NE cells after intraperitoneal injection of FG-4592 in *Cgrp- tdTomato* reporter mice (n=6). (E) Quantification of tdTomato+ solitary NE cells per trachea from vehicle or FG4592-treated *Cgrp-tdTomato* mice (*n*=6). (F) Schematic representation of cobalt chloride induction of NE cell differentiation and subsequent labeling of tdTomato^{+} cells in *Cgrp-tdTomato* reporter mice. (G) Whole-mount tracheal images showing an increase in the number of tdTomato^{+} solitary NE cells after intranasal administration of cobalt chloride in *Cgrp-tdTomato* reporter mice (*n*=6). (H) Quantification of tdTomato+ cells per trachea from vehicle or $CoCl_2$ administered *Cgrp-tdTomato* mice (*n*=6). *** $p<0.001$ and ** $p<0.01$ or * $p<0.05$; error bars, means ± standard deviation. Scale bars 300 μm.

Fig. S8.

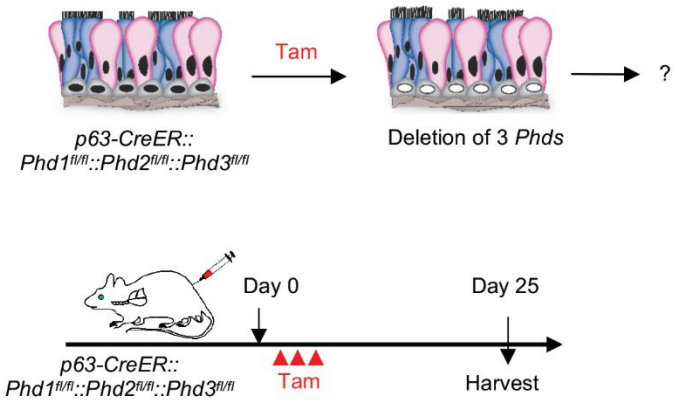

Fig. S8. (A) Schematic of protocol for simultaneous deletion of all 3 prolyl hydroxylases from basal stem cells using *p63-CreER::PhDs* mice.

Fig. S9.

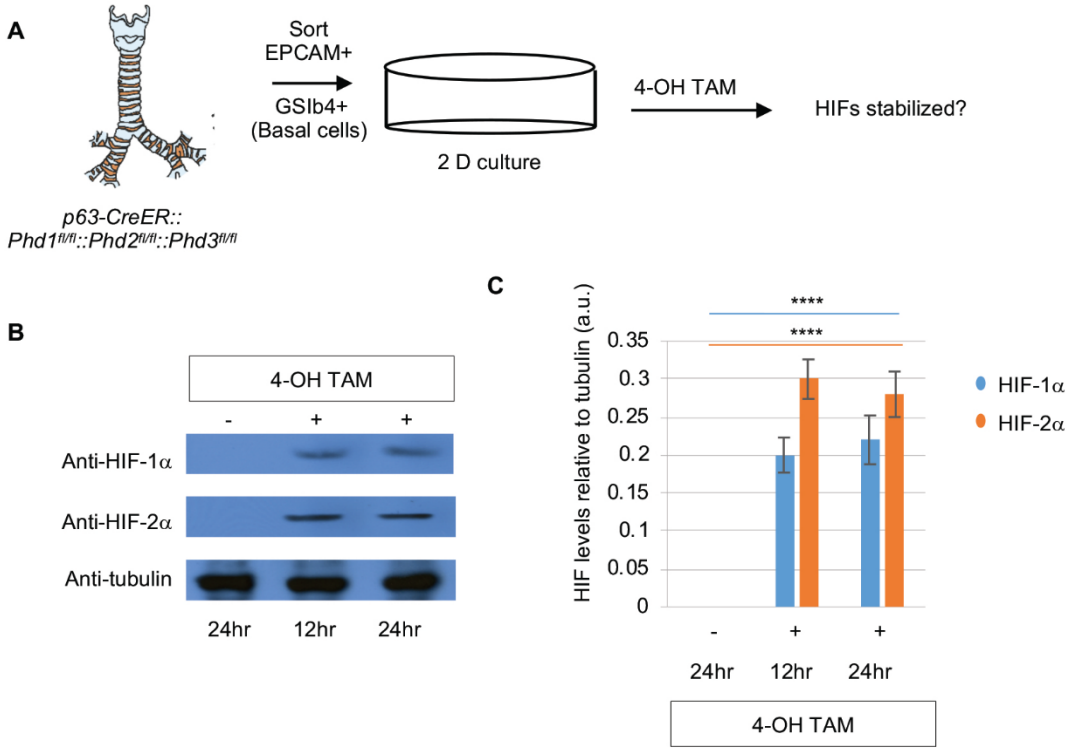

Fig. S9. Deletion of Prolyl hydroxylases from basal stem cells stabilizes HIF-1α and HIF-2α in 2D culture.

(A) Schematic representation of mouse tracheal basal stem cell isolation from *p63-CreER::Phd1*$^{fl/fl}$*::Phd2*$^{fl/fl}$*::Phd3*^{fl} mouse and treatment of 4-hydroxytamoxifen (4-OH TAM) to delete all three hydroxylases in 2D culture. (B) Western blot analysis of HIF-1α (120 kDa) (top row), HIF-2α (118 kDa) (middle row), and tubulin (50 kDa) (loading control) (bottom row) in

basal stem cells. C) Quantification of HIF-1α and HIF-2α, western blot signal from (B). ****p <0.0001; error bars, means ± standard deviation. a.u.=arbitrary units.

Fig. S10.

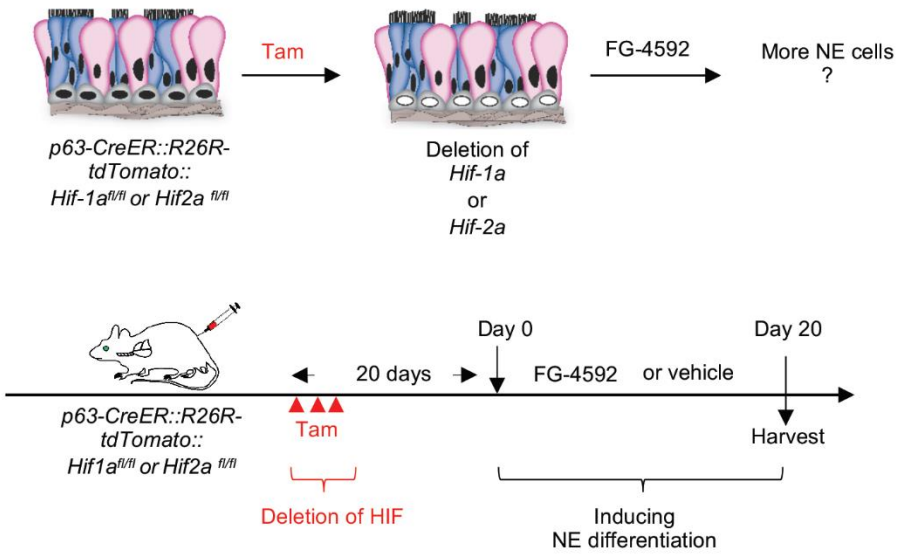

Fig. S10. Schematic representation of deletion of *Hif1α* or *Hif2α* from basal cells in p63-*Hif1α* or p63-*Hif2α* mice followed by FG-4592-induced NE differentiation.

Fig. S11.

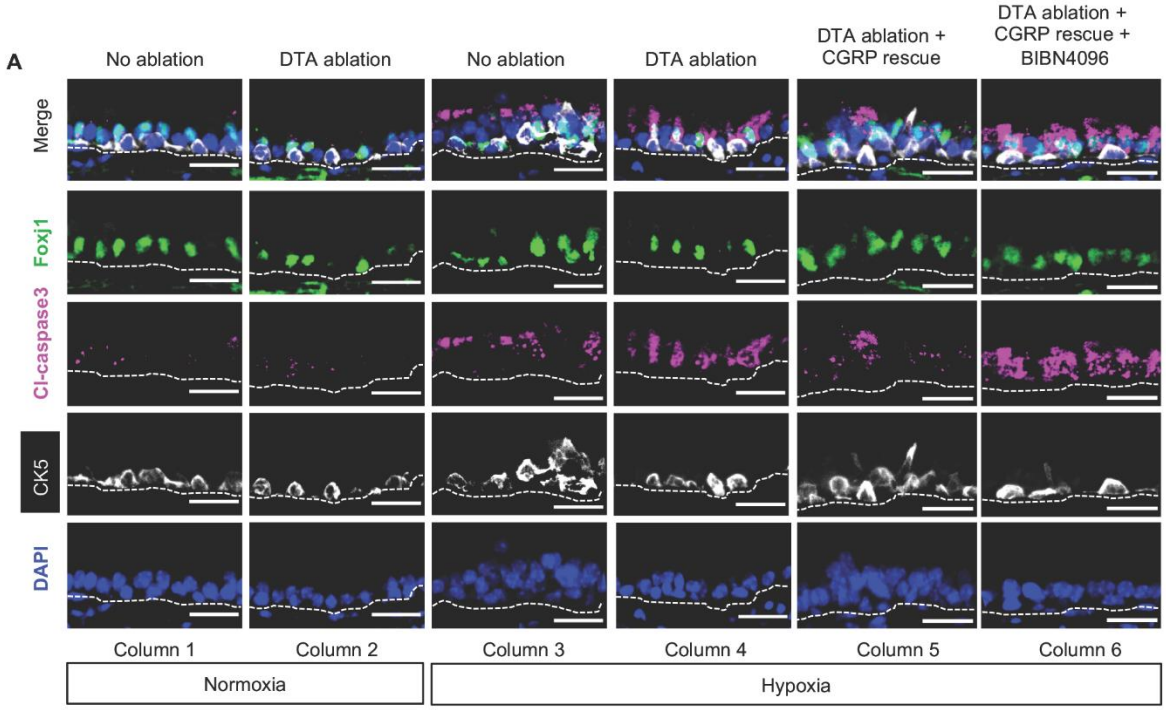
A
No ablation
DTA ablation
No ablation
DTA ablation
DTA ablation + CGRP rescue
DTA ablation + CGRP rescue + BIBN4096
Merge
Foxj1
Cl-caspase3
CK5
DAPI
Column 1
Column 2
Column 3
Column 4
Column 5
Column 6
Normoxia
Hypoxia

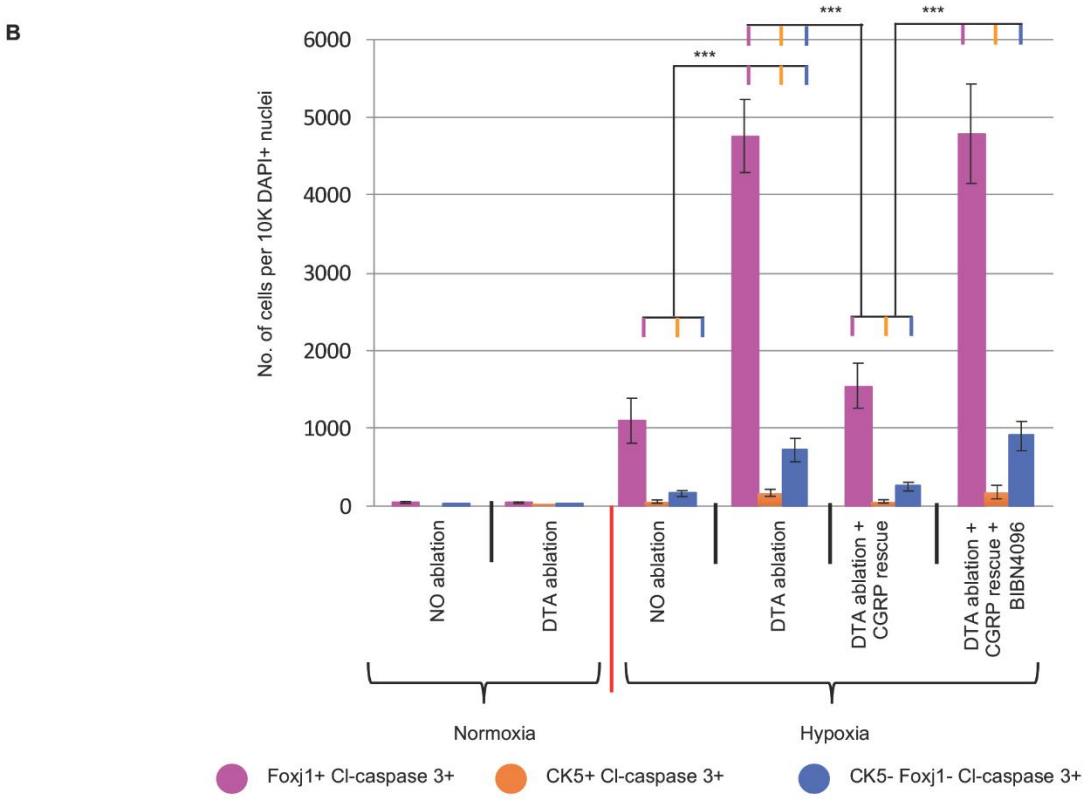
B
No. of cells per 10K DAPI+ nuclei
6000
5000
4000
3000
2000
1000
0
***
***
***
NO ablation
DTA ablation
NO ablation
DTA ablation
DTA ablation + CGRP rescue
DTA ablation + CGRP rescue + BIBN4096
Normoxia
Hypoxia
Foxj1+ Cl-caspase 3+
CK5+ Cl-caspase 3+
CK5- Foxj1- Cl-caspase 3+

Fig. S11. Solitary NE cells prevent epithelial apoptosis during hypoxia.

(A) Immunostaining for Foxj1 (green), Cl-caspase-3 (magenta) and CK5 (white) on normoxic and hypoxic tracheal epithelium with or without NE cell ablation (*Cgrp-CreER:: R26R-DTA* background), and with CGRP administration or blockade. (B) Quantification of Foxj1 (green), Cl-caspase-3 (magenta) and CK5 (white) cells in normoxic and hypoxic tracheal epithelium prior to and following NE cell ablation and with CGRP administration or blockade (n=5). Scale bars 30 μm, unless indicated. *** p<0.001 and ** p <0.01 or * p <0.05; error bars, means ± standard deviation.

Fig. S12.

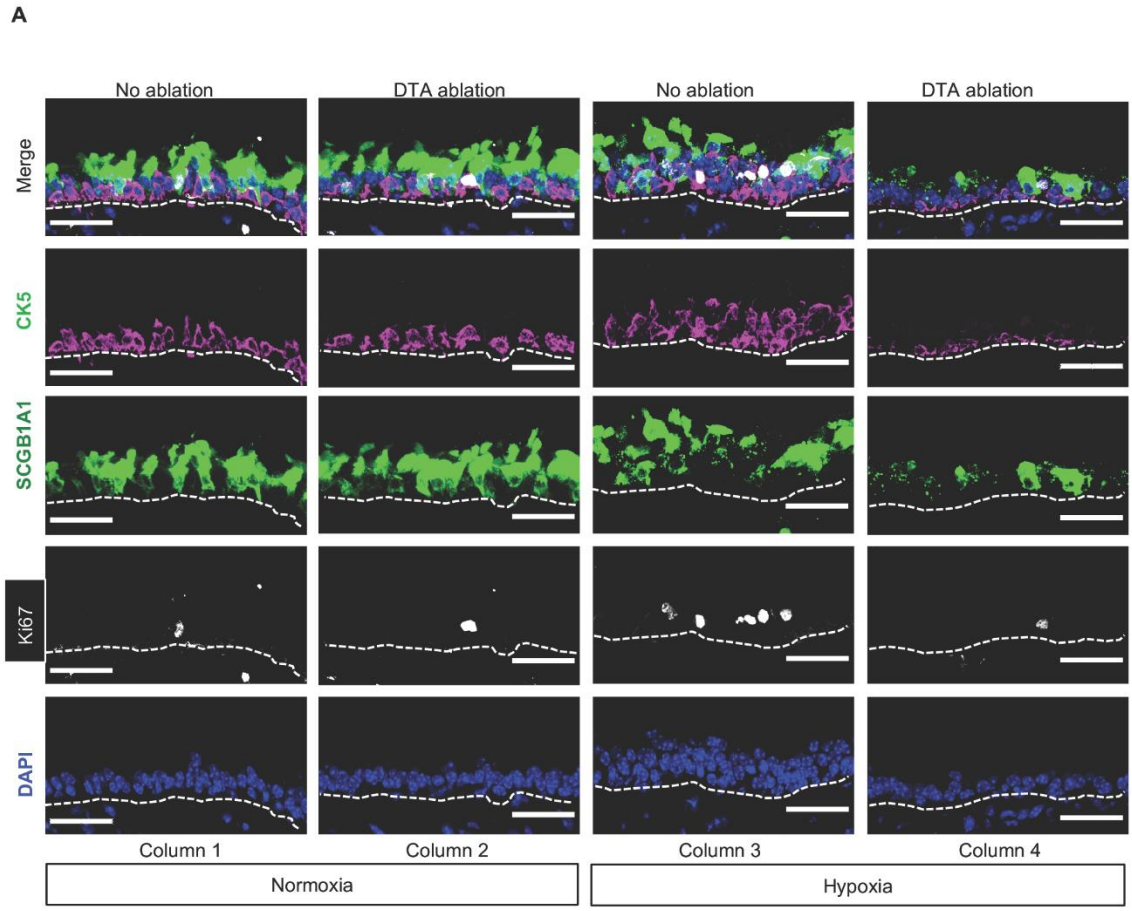
A
No ablation
DTA ablation
No ablation
DTA ablation
Merge
CK5
SCGB1A1
Ki67
DAPI
Column 1
Column 2
Column 3
Column 4
Normoxia
Hypoxia

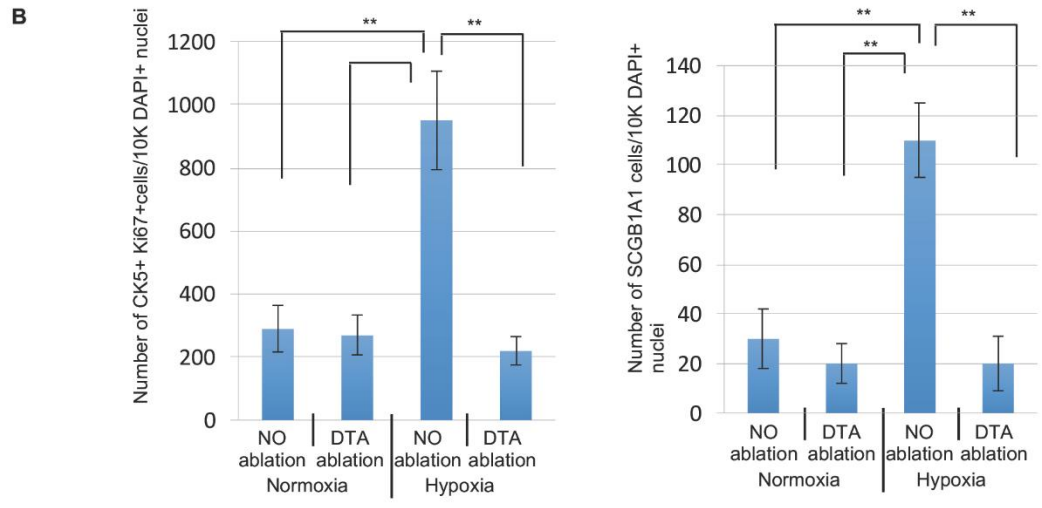
B
Number of CK5+ Ki67+cells/10K DAPI+ nuclei
1200
1000
800
600
400
200
0
**
**
NO ablation
DTA ablation
NO ablation
DTA ablation
Normoxia
Hypoxia
Number of SCGB1A1 cells/10K DAPI+ nuclei
140
120
100
80
60
40
20
0
**
**
**
NO ablation
DTA ablation
NO ablation
DTA ablation
Normoxia
Hypoxia

Fig. S12. Solitary NE cell ablation reduces hypoxia-induced secretory and basal stem cell replication.

(A) Immunostaining for CK5 (magenta), SCGB1A1 (green) and Ki67 (white) on normoxic and hypoxic tracheal epithelium with and without NE cell ablation (*Cgrp-CreER:: R26R-DTA* background). (B) Quantification of $CK5^+$ $Ki67^+$ and $SCGB1A1^+$ $Ki67^+$cells in normoxic and hypoxic tracheal epithelium from (A). (n=5). ** p <0.01; error bars, means ± standard deviation. Scale bars 30 μm, unless indicated.

Fig. S13.

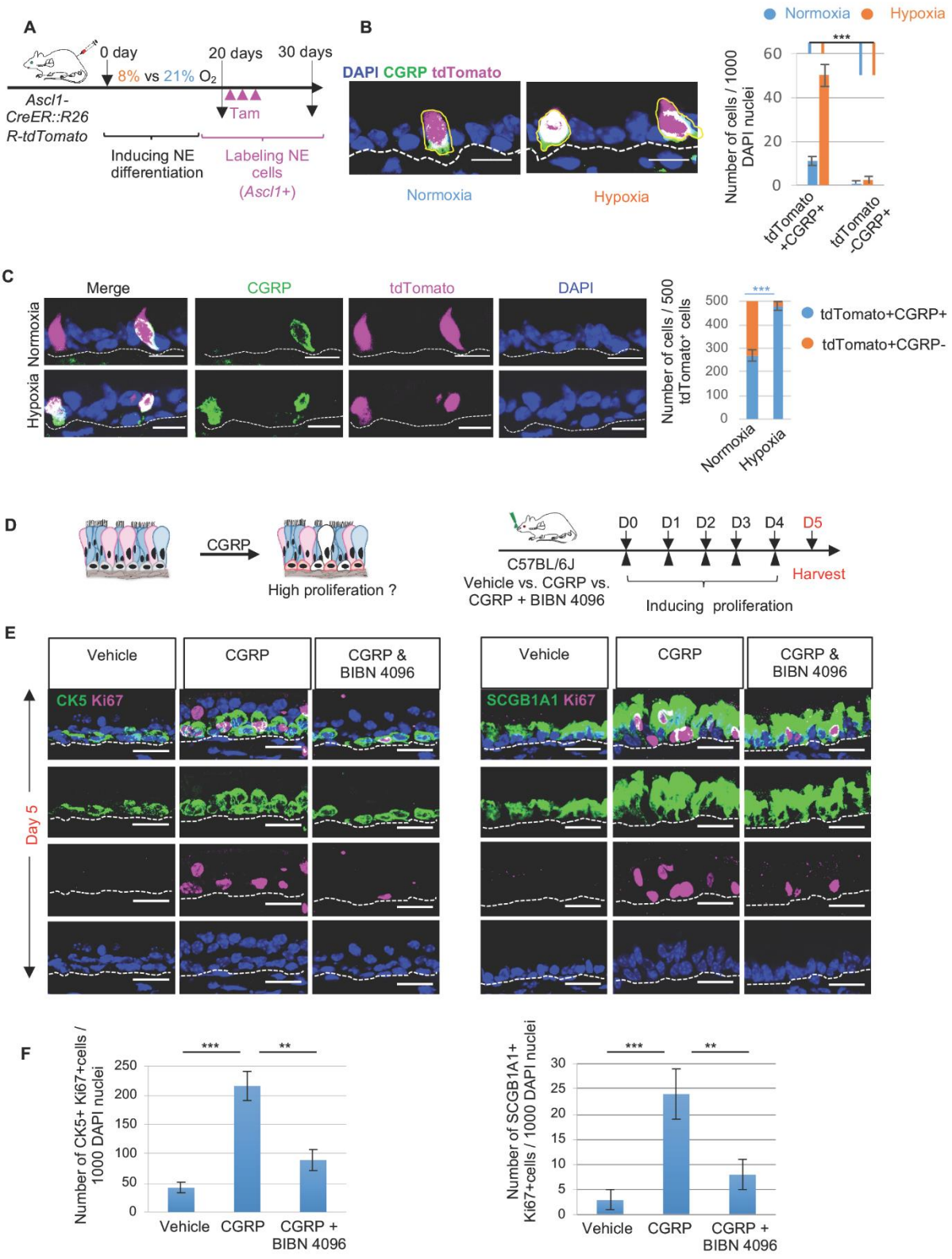
A
0 day
20 days
30 days
8% vs 21% O2
Tam
Ascl1-CreER::R26 R-tdTomato
Inducing NE differentiation
Labeling NE cells (Ascl1+)
B
DAPI CGRP tdTomato
Normoxia
Hypoxia
Normoxia
Hypoxia
***
Number of cells / 1000 DAPI nuclei
tdTomato +CGRP+
tdTomato -CGRP+
C
Merge
CGRP
tdTomato
DAPI
Normoxia
Hypoxia
***
Number of cells / 500 tdTomato+ cells
tdTomato+CGRP+
tdTomato+CGRP-
Normoxia
Hypoxia
D
CGRP
High proliferation ?
C57BL/6J
Vehicle vs. CGRP vs. CGRP + BIBN 4096
D0
D1
D2
D3
D4
D5
Harvest
Inducing proliferation
E
Vehicle
CGRP
CGRP & BIBN 4096
CK5 Ki67
SCGB1A1 Ki67
Day 5
F
***
**
Number of CK5+ Ki67+cells / 1000 DAPI nuclei
Vehicle
CGRP
CGRP + BIBN 4096
Number of SCGB1A1+ Ki67+cells / 1000 DAPI nuclei

Fig. S13. Solitary NE cells produce CGRP, which induces cell proliferation in the adult tracheal epithelium.

(A) Schematic representation of induction of NE differentiation and subsequent labeling of *Ascl1*$^{+}$ solitary NE cells using *Ascl1-tdTomato* reporter mice. (B) Immunostaining for CGRP (green) on normoxic and hypoxic tracheal epithelium from *Ascl1-tdTomato* lineage labeled mice (*n*=8) and quantification of CGRP expression in tdTomato^{+} cells. (C) Immunostaining for CGRP (green) on normoxic and hypoxic tracheal epithelium from *Ascl1-tdTomato* lineage labeled mice (*n*=8) and quantification of lineage labeled cells expressing CGRP (tissue samples from Fig. 2A). (D) Schematic representation of CGRP and combined CGRP+BIBN 4096 intranasal administration to wild type mice. (E) Immunostaining for CK5 (green), SCGB1A1 (green), and Ki67 (magenta) of CGRP-treated and BIBN 4096-treated trachea (*n*=4). (F) Quantification of CK5+Ki67+ and SCGB1A1+Ki67+ cells from CGRP and BIBN-4096 treated mice (*n*=4). *** $p<0.001$ and ** $p<0.01$ error bars, means ± standard deviation. Scale bars 30 μm.

Fig. S14.

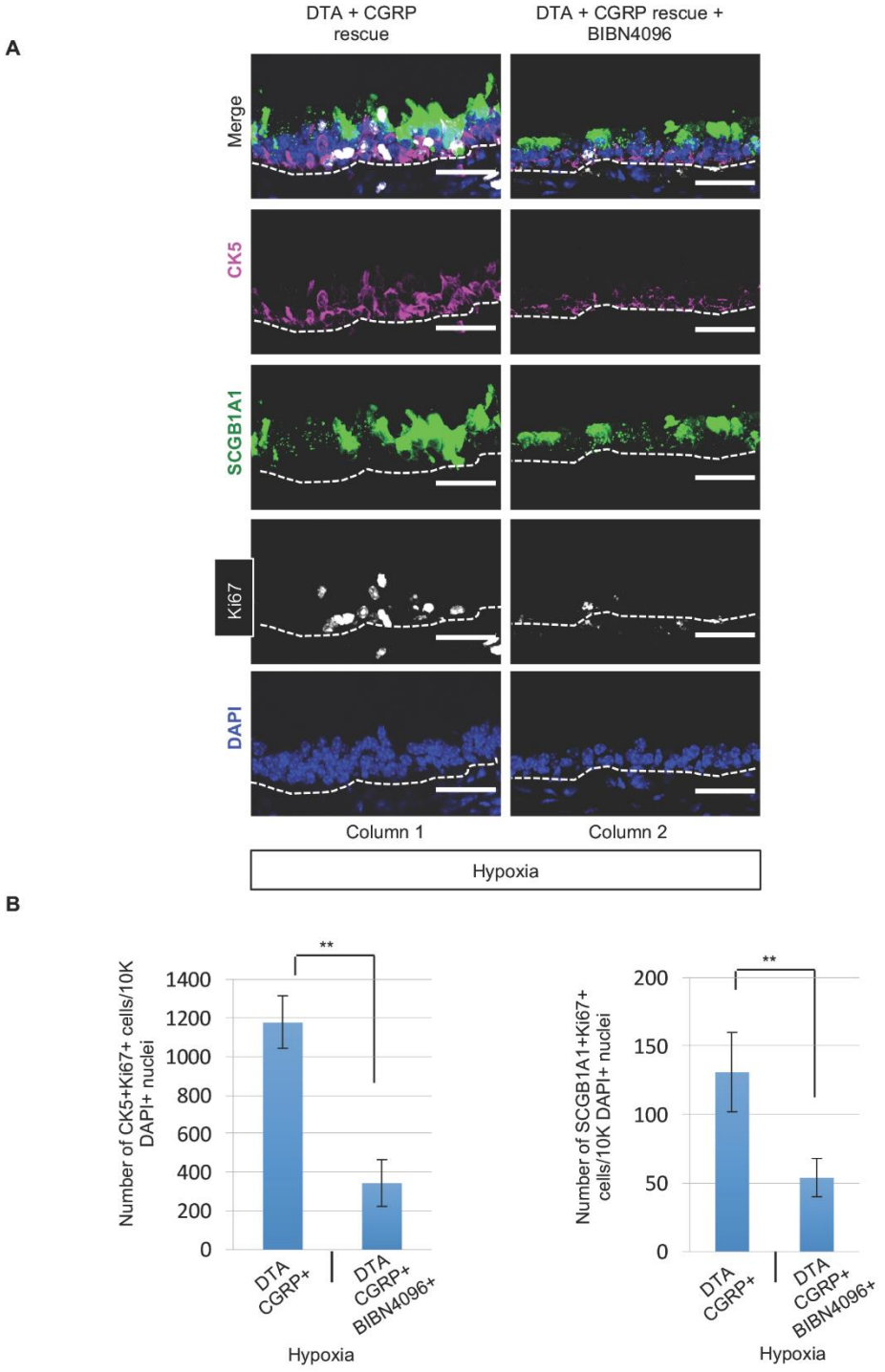
A
DTA + CGRP rescue
DTA + CGRP rescue + BIBN4096
Merge
CK5
SCGB1A1
Ki67
DAPI
Column 1
Column 2
Hypoxia
B
Number of CK5+Ki67+ cells/10K DAPI+ nuclei
1400
1200
1000
800
600
400
200
0
**
DTA CGRP+
DTA CGRP+ BIBN4096+
Hypoxia
Number of SCGB1A1+Ki67+ cells/10K DAPI+ nuclei
200
150
100
50
0
**
DTA CGRP+
DTA CGRP+ BIBN4096+
Hypoxia

Fig. S14. CGRP rescues the defect in proliferation caused by solitary NE cell ablation

(A) Immunostaining for CK5 (magenta), SCGB1A1 (green) and Ki67 (white) on hypoxia-treated mice with and without NE cell ablation (*Cgrp-CreER:: R26R-DTA* background) and with CGRP rescue or CGRP blockade. (B) Quantification of $CK5^+$ $Ki67^+$ and $SCGB1A1^+$ $Ki67^+$cells from hypoxia-treated mice with and without NE cell ablation and with CGRP rescue or CGRP blockade. (n=5). ** p <0.01; error bars, means ± standard deviation. Scale bars 30 μm, unless indicated.

Fig.S15.

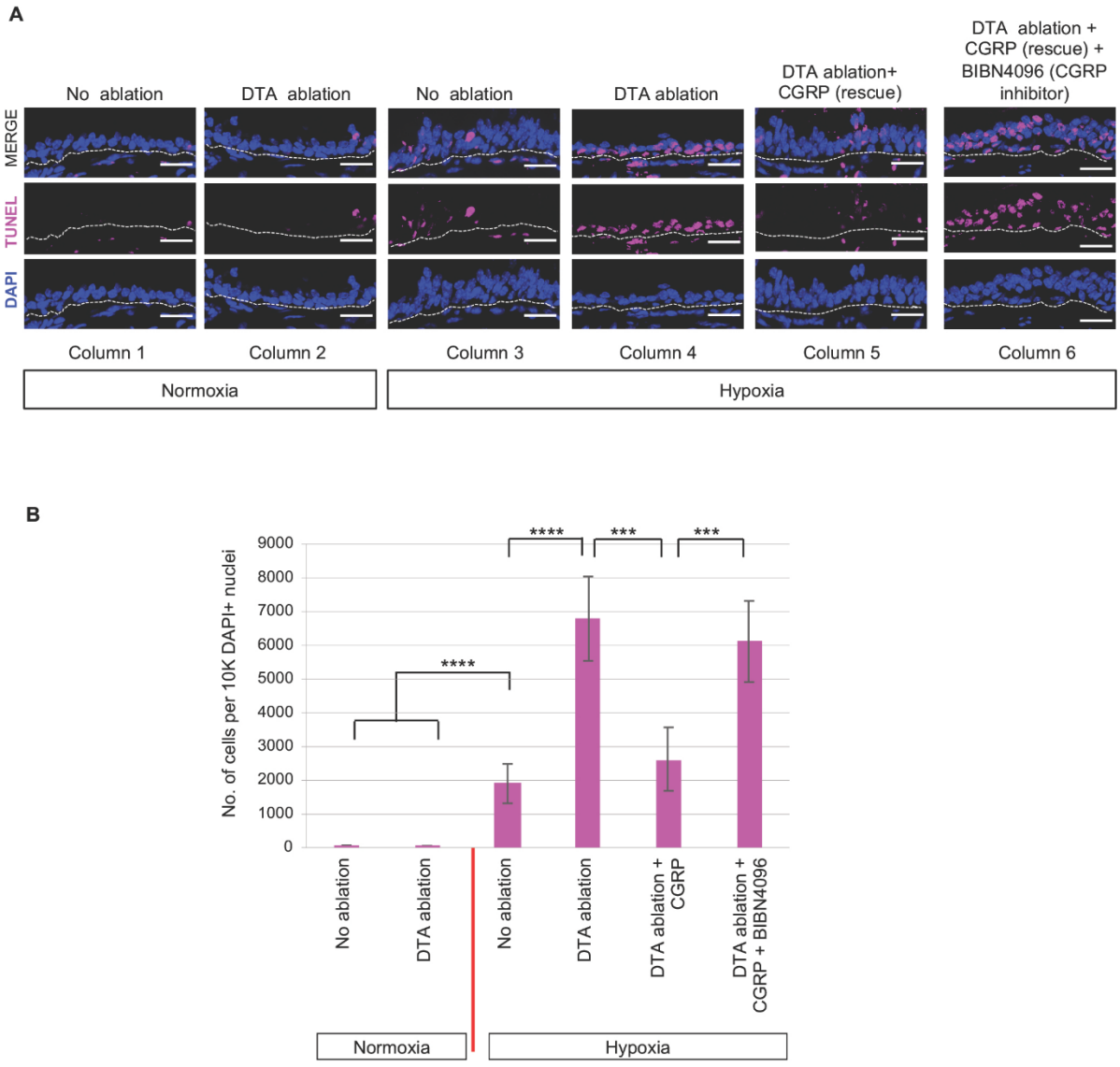
A
No ablation
DTA ablation
No ablation
DTA ablation
DTA ablation+ CGRP (rescue)
DTA ablation + CGRP (rescue) + BIBN4096 (CGRP inhibitor)
MERGE
TUNEL
DAPI
Column 1
Column 2
Column 3
Column 4
Column 5
Column 6
Normoxia
Hypoxia
B
No. of cells per 10K DAPI+ nuclei
9000
8000
7000
6000
5000
4000
3000
2000
1000
0
****
****
***
***
No ablation
DTA ablation
No ablation
DTA ablation
DTA ablation + CGRP
DTA ablation + CGRP + BIBN4096
Normoxia
Hypoxia

Fig. S15. TUNEL assay demonstrates that solitary NE cells prevent epithelial cell apoptosis

(A) Immunostaining to detect apoptotic cells by TUNEL assay (magenta) on normoxic and hypoxic tracheal epithelium with and without NE cell ablation (*Cgrp-CreER:: R26R-DTA* background) and with CGRP rescue and CGRP receptor inhibitor. (B) Quantification of apoptotic cells under normoxic or hypoxic conditions with and without NE cell ablation and with CGRP administration or blockade (n=5). **** p<0.0001 and *** p <0.001; error bars, means ± standard deviation. Scale bars 30 μm, unless indicated.

Fig. S16.

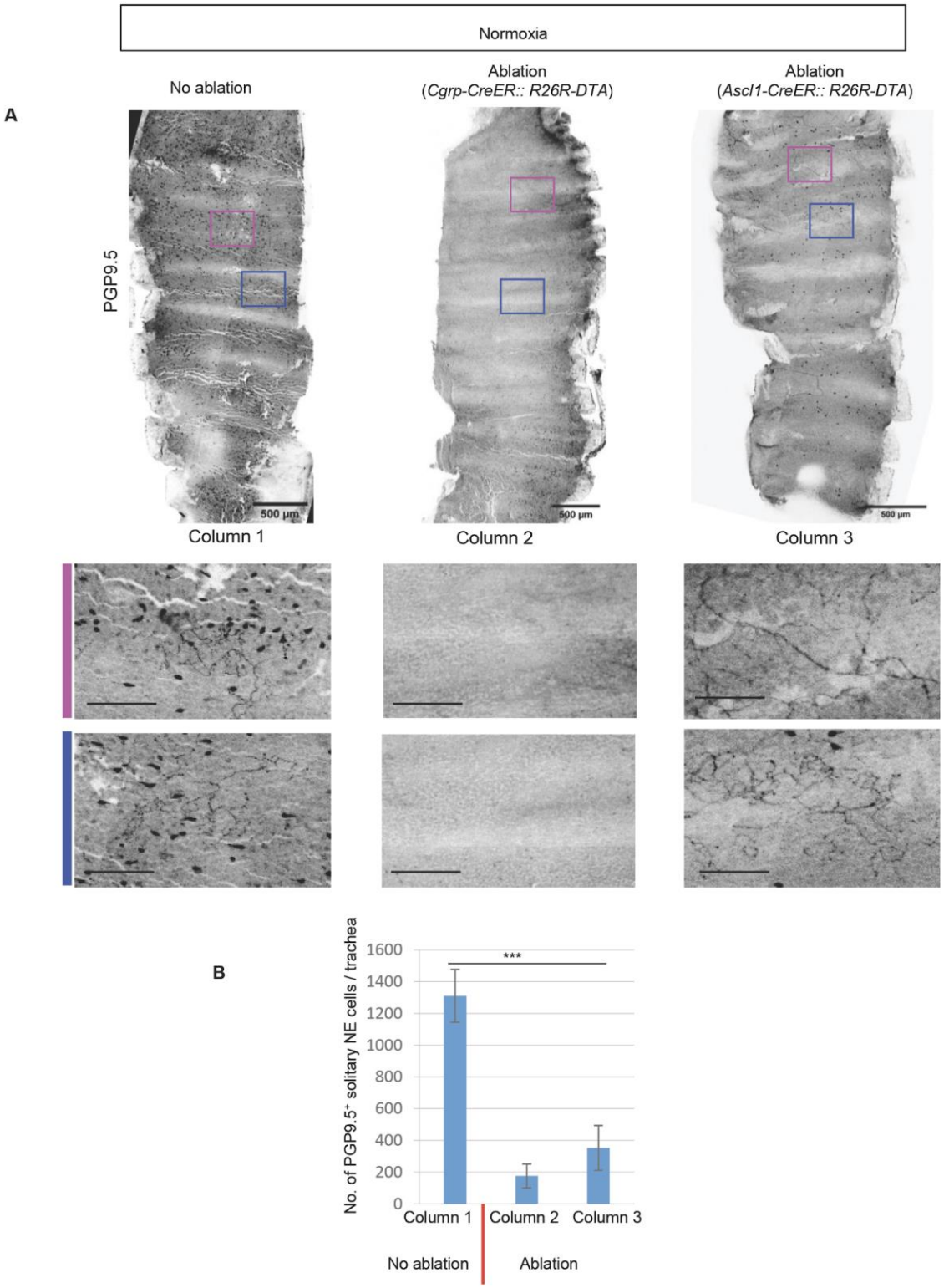
Normoxia
No ablation
Ablation
(Cgrp-CreER:: R26R-DTA)
Ablation
(Ascl1-CreER:: R26R-DTA)
A
PGP9.5
500 µm
Column 1
Column 2
Column 3
B
No. of PGP9.5+ solitary NE cells / trachea
1600
1400
1200
1000
800
600
400
200
0
***
Column 1
Column 2
Column 3
No ablation
Ablation

Fig. S16. Comparison of NE cell and nerve ablation in tracheal epithelium using *Cgrp-CreER* and *Ascl1-CreER* driver lines.

(A) Immunostaining for PGP9.5 on normoxic whole-mount trachea with and without NE cell ablation. Left panel; no ablation, middle panel; NE cell ablation using *Cgrp-CreER:: R26R-DTA* driver, and right panel; NE cell ablation using *Ascl1-CreER:: R26R-DTA* driver line. Two areas (magenta and blue boxes) in each panel are magnified for clarity. Both models result in the efficient ablation of NE cells but the *Ascl1-CreER* driver spares neurons (B) Quantification of $PGP9.5^{+}$ cells from normoxic whole-mount trachea with and without NE cell ablation. *** $p < 0.001$; error bars, means ± standard deviation. Scale bars 50 μm, unless indicated.

Fig. S17.

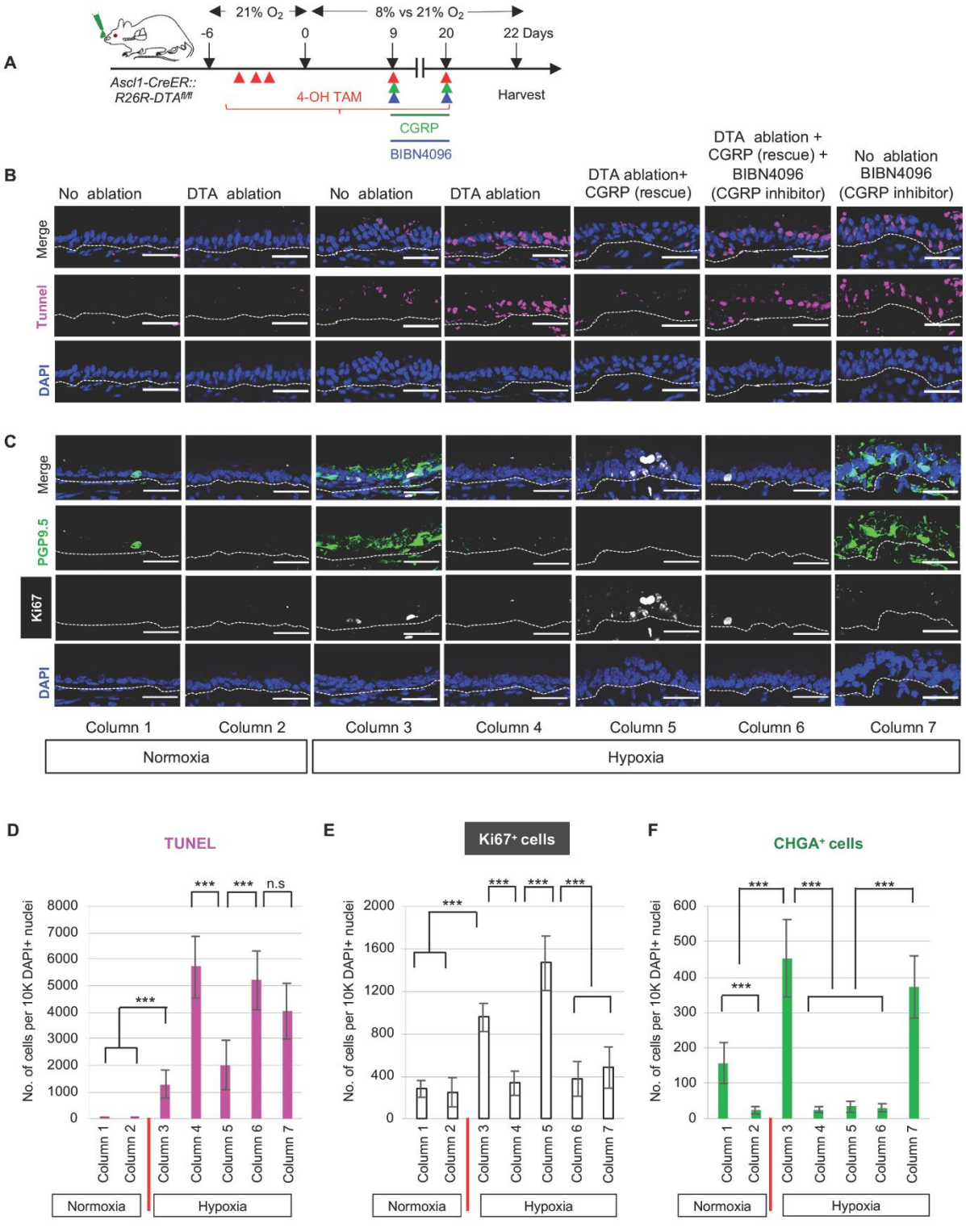
A
21% O2
8% vs 21% O2
-6
0
9
20
22 Days
Ascl1-CreER::
R26R-DTAfl/fl
4-OH TAM
Harvest
CGRP
BIBN4096
B
No ablation
DTA ablation
No ablation
DTA ablation
DTA ablation+
CGRP (rescue)
DTA ablation +
CGRP (rescue) +
BIBN4096
(CGRP inhibitor)
No ablation
BIBN4096
(CGRP inhibitor)
Merge
Tunnel
DAPI
C
Merge
PGP9.5
Ki67
DAPI
Column 1
Column 2
Column 3
Column 4
Column 5
Column 6
Column 7
Normoxia
Hypoxia
D
TUNEL
No. of cells per 10K DAPI+ nuclei
***
***
n.s
***
E
Ki67+ cells
No. of cells per 10K DAPI+ nuclei
***
***
***
***
F
CHGA+ cells
No. of cells per 10K DAPI+ nuclei
***
***
***
***

Fig. S17. Solitary NE cells are required for the repair of hypoxia-induced injury demonstrated using the nerve-sparing *Ascl1* driver line.

(A) Schematic representation of NE cell ablation to assess the functional consequences of NE cell loss in the setting of hypoxia-induced injury. (B) Immunostaining to detect apoptotic cells by TUNEL assay (magenta) on normoxic and hypoxic tracheal epithelium with and without NE cell ablation and with CGRP rescue and CGRP receptor inhibitor. (C) Immunostaining for CHGA (green), and Ki67 (white) on normoxic and hypoxic tracheal epithelium with and without NE cell ablation and with CGRP rescue and CGRP receptor inhibitor. Quantification of (D) $TUNEL^+$ cells, (E) $Ki67^+$, and (E) $CHGA^+$ cells under normoxic or hypoxic conditions with and without NE cell ablation and with CGRP administration or blockade (n=5). n.s. = not significant, *** p<0.001; error bars, means ± standard deviation. Scale bars 30 μm, unless indicated.

Fig. S18.

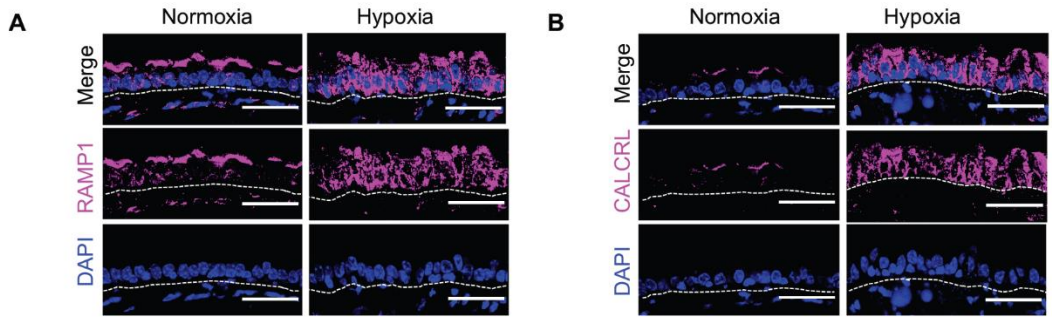

Fig. S18. Upregulation of CGRP receptor expression in the airway epithelium following hypoxia. Immunostaining for RAMP1 (A) and CALCRL (B) on normoxic and hypoxic tracheal epithelium. Both antibodies have a high non-specific background in normoxia.

Fig. S19.

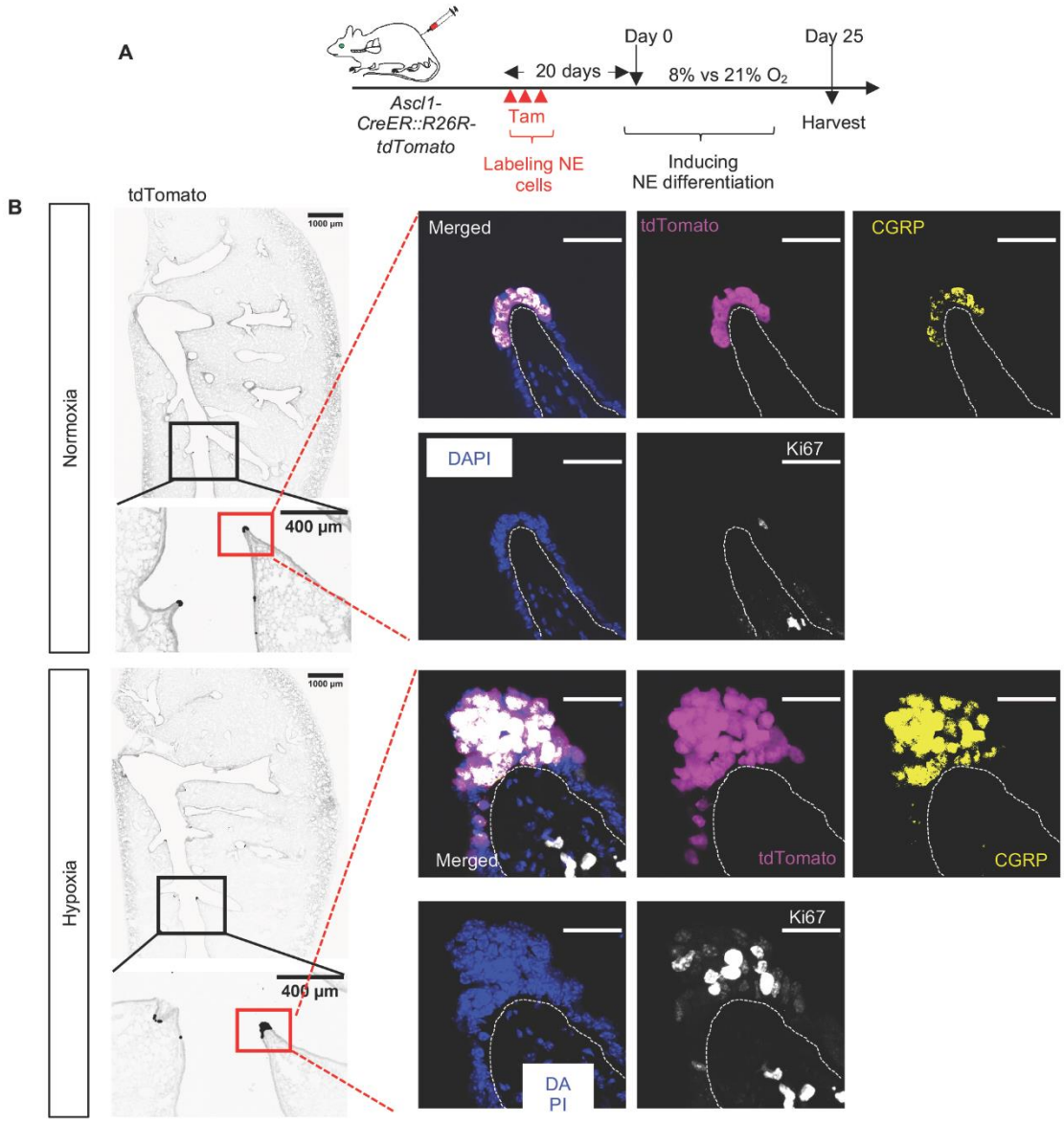
A
Day 0
Day 25
20 days
8% vs 21% O2
Ascl1-CreER::R26R-tdTomato
Tam
Harvest
Labeling NE cells
Inducing NE differentiation
B
tdTomato
Normoxia
Hypoxia
1000 μm
400 μm
Merged
tdTomato
CGRP
DAPI
Ki67
DA PI
C
N.S
**
No. of NEBs / left lobe of the lung
tdTomato + CGRP + Ki67-
tdTomato + CGRP + Ki67+
tdTomato - CGRP +
Normoxia
Hypoxia
D
*
Average area (μm²) of NEBs

Fig. S19. NEB hyperplasia stimulated by hypoxia.

(A) Schematic representation of labeling of *Ascl1*$^{+}$ NEBs using *Ascl1-tdTomato* reporter mice and subsequent exposure to hypoxia. (B) Black and white panels are low magnification images of the left lobe of the lung, normoxia (upper left) and hypoxia (lower left). The red boxed regions are enlarged in the right panel and show immunostaining for CGRP (yellow) and Ki67 (white) on sections from *Ascl1-tdTomato* reporter mice during normoxia or hypoxia. Quantification of tdTomato+CGRP+Ki67-, tdTomato+CGRP+Ki67+, and tdTomato-CGRP+ NEBs numbers (C) and average area (μm^2) of NEBs (D) during normoxia or hypoxia (n=5). n.s.=not significant, ** $p<0.01$, and * $p<0.05$; error bars, means ± standard deviation. Scale bars 30 μm, unless indicated.

Fig. S20.

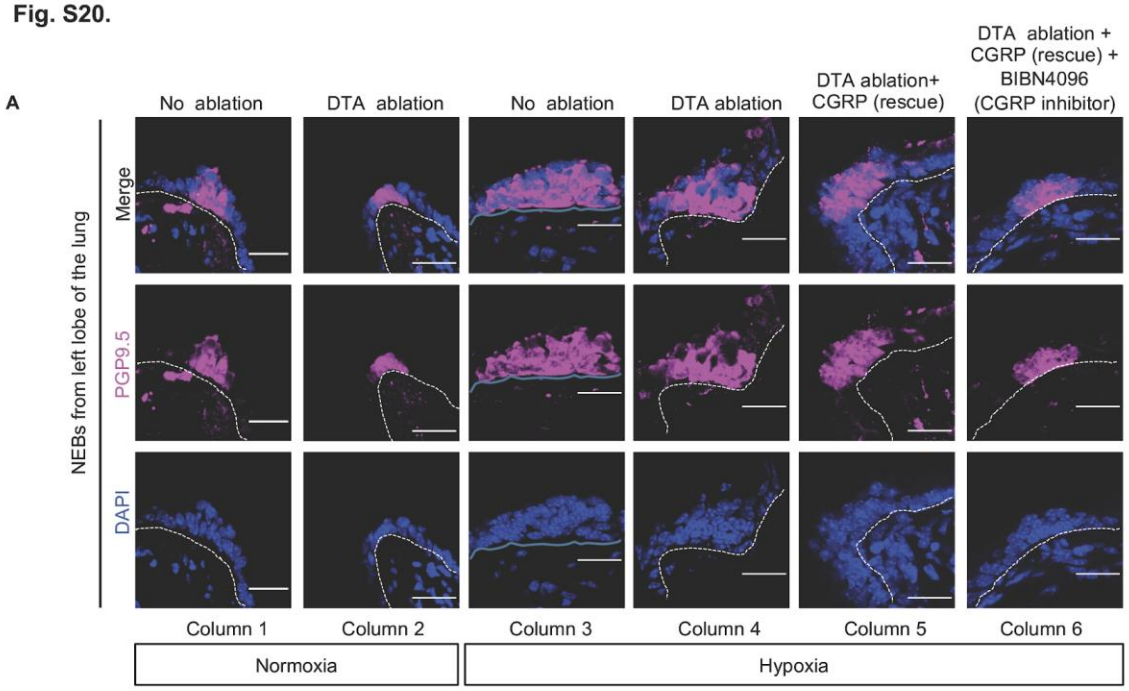
A
No ablation
DTA ablation
No ablation
DTA ablation
DTA ablation+ CGRP (rescue)
DTA ablation + CGRP (rescue) + BIBN4096 (CGRP inhibitor)
NEBs from left lobe of the lung
Merge
PGP9.5
DAPI
Column 1
Column 2
Column 3
Column 4
Column 5
Column 6
Normoxia
Hypoxia

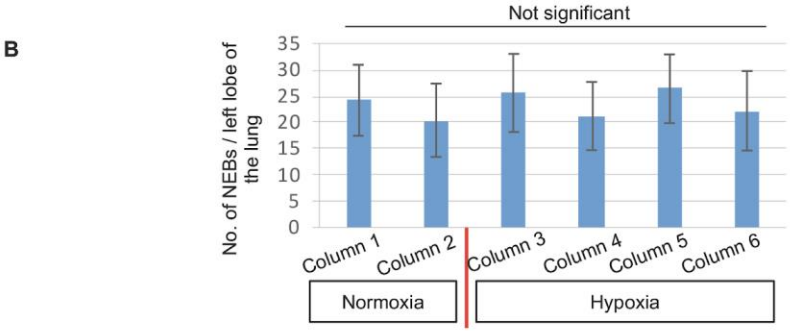
B
Not significant
No. of NEBs / left lobe of the lung
35
30
25
20
15
10
5
0
Column 1
Column 2
Column 3
Column 4
Column 5
Column 6
Normoxia
Hypoxia

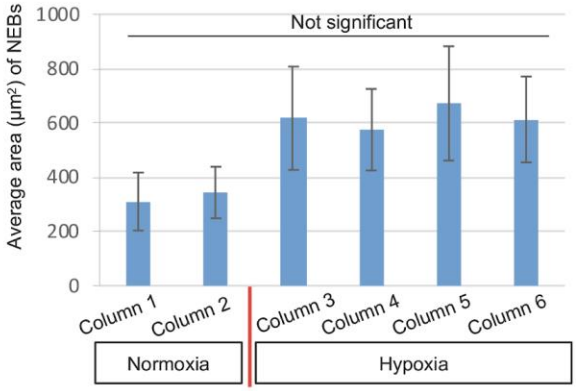
Not significant
Average area (μm²) of NEBs
1000
800
600
400
200
0
Column 1
Column 2
Column 3
Column 4
Column 5
Column 6
Normoxia
Hypoxia

Fig. S20. NEBs were preserved despite genetic ablation of tracheal solitary NE cells.

(A) Immunostaining for PGP9.5 to detect NEBs following NE cell ablation coupled to hypoxia and CGRP rescue or blockade. (B) Upper panel, quantification of NEBs from normoxic and hypoxic lung with and without NE cell ablation (*Cgrp-CreERT2::Rosa26-DTA* background*)* and with CGRP rescue and CGRP receptor inhibitors (n=5) and lower panel, quantification of average area (μm2) of NEBs. error bars, means ± standard deviation. Scale bars 30 μm, unless indicated.

Fig. S21.

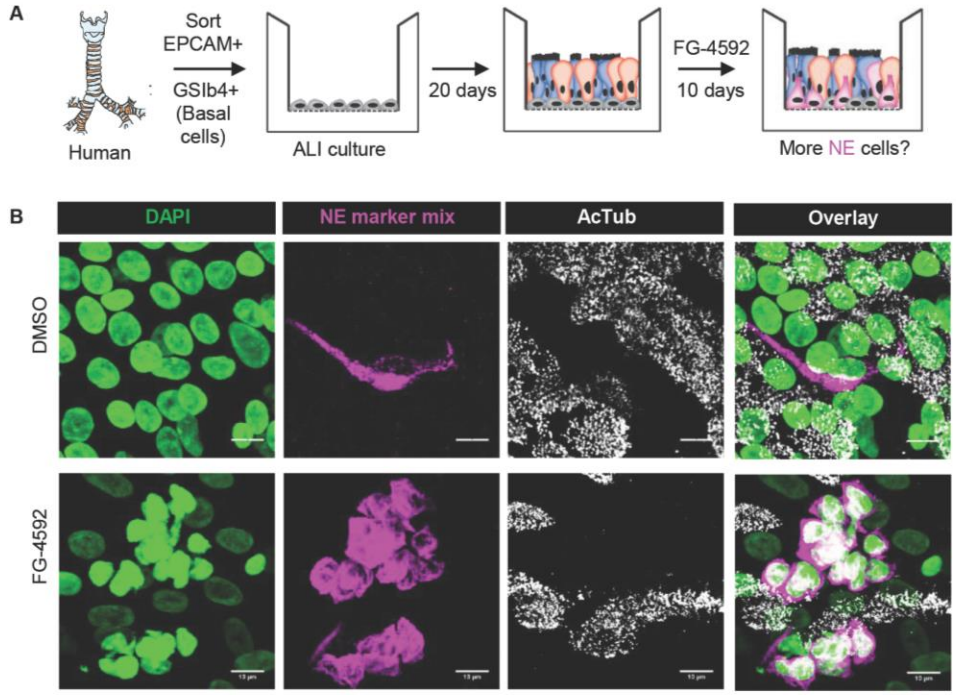
A
Human
Sort
EPCAM+
GSIb4+
(Basal
cells)
ALI culture
20 days
FG-4592
10 days
More NE cells?
B
DAPI
NE marker mix
AcTub
Overlay
DMSO
FG-4592

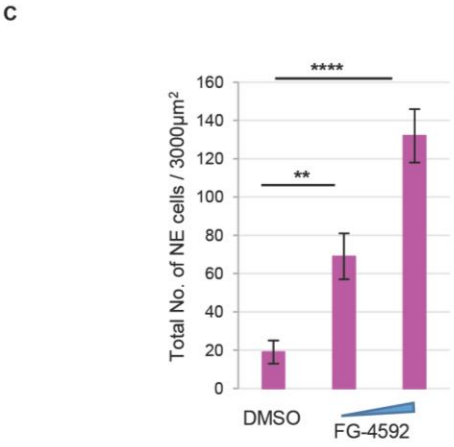
C
Total No. of NE cells / 3000μm²
160
140
120
100
80
60
40
20
0
****
**
DMSO
FG-4592

Fig. S21. FG-4592 induces NE cell differentiation in human airway epithelium.

(A) Schematic representation of human bronchial basal cell isolation and induction of NE cell differentiation in ALI culture. (B) Immunostaining for NE cells using a panel of NE cell antibodies (magenta) and ciliated cell maker acetylated tubulin (white). (C) Quantification of human NE cells in airway epithelial cultures treated with FG-4592 (n=2). n= biological replicates/condition repeated three times (three independent experiments). *** p<0.001 and ** p <0.01; error bars, means ± standard deviation. Scale bars 10 μm, unless indicated.

References and Notes

1. F. Feyrter, Zur Normung der Silberimpragnation neuraler und nichtneuraler Gewe. *Virchows Arch. Pathol. Anat. Physiol.* **320**, 551–563 (1951). doi:10.1007/BF01880688

2. F. Feyrter, Zur Pathologie des argyrophilen Helle-ZellenOrganes im Bronchialbaum des Menschen. *Virchows Arch. Pathol. Anat. Physiol. Med.* **325**, 723–732 (1954). doi:10.1007/BF00955103

3. E. Cutz, Hyperplasia of pulmonary neuroendocrine cells in infancy and childhood. *Semin. Diagn. Pathol.* **32**, 420–437 (2015). doi:10.1053/j.semdp.2015.08.001 Medline

4. E. Cutz, H. Yeger, J. Pan, T. Ito, Pulmonary Neuroendocrine Cell System in Health and Disease. *Curr. Respir. Med. Rev.* **4**, 174–186 (2008). doi:10.2174/157339808785161314

5. M. Noguchi, K. Sumiyama, M. Morimoto, Directed Migration of Pulmonary Neuroendocrine Cells toward Airway Branches Organizes the Stereotypic Location of Neuroepithelial Bodies. *Cell Rep.* **13**, 2679–2686 (2015). doi:10.1016/j.celrep.2015.11.058 Medline

6. C. S. Kuo, M. A. Krasnow, Formation of a Neurosensory Organ by Epithelial Cell Slithering. *Cell* **163**, 394–405 (2015). doi:10.1016/j.cell.2015.09.021 Medline

7. E. Cutz, A. Jackson, Neuroepithelial bodies as airway oxygen sensors. *Respir. Physiol.* **115**, 201–214 (1999). doi:10.1016/S0034-5687(99)00018-3 Medline

8. R. I. Linnoila, Functional facets of the pulmonary neuroendocrine system. *Lab. Invest.* **86**, 425–444 (2006). doi:10.1038/labinvest.3700412 Medline

9. E. Cutz, J. Pan, H. Yeger, N. J. Domnik, J. T. Fisher, Recent advances and contraversies on the role of pulmonary neuroepithelial bodies as airway sensors. *Semin. Cell Dev. Biol.* **24**, 40–50 (2013). doi:10.1016/j.semcdb.2012.09.003 Medline

10. K. Branchfield, L. Nantie, J. M. Verheyden, P. Sui, M. D. Wienhold, X. Sun, Pulmonary neuroendocrine cells function as airway sensors to control lung immune response. *Science* **351**, 707–710 (2016). doi:10.1126/science.aad7969 Medline

11. S. D. Reynolds, K. U. Hong, A. Giangreco, G. W. Mango, C. Guron, Y. Morimoto, B. R. Stripp, Conditional clara cell ablation reveals a self-renewing progenitor function of pulmonary neuroendocrine cells. *Am. J. Physiol. Lung Cell. Mol. Physiol.* **278**, L1256–L1263 (2000). doi:10.1152/ajplung.2000.278.6.L1256 Medline

12. X. Gu, P. H. Karp, S. L. Brody, R. A. Pierce, M. J. Welsh, M. J. Holtzman, Y. Ben-Shahar, Chemosensory functions for pulmonary neuroendocrine cells. *Am. J. Respir. Cell Mol. Biol.* **50**, 637–646 (2014). doi:10.1165/rcmb.2013-0199OC Medline

13. Y. Ouadah, E. R. Rojas, D. P. Riordan, S. Capostagno, C. S. Kuo, M. A. Krasnow, Rare Pulmonary Neuroendocrine Cells Are Stem Cells Regulated by Rb, p53, and Notch. *Cell* **179**, 403–416.e23 (2019). doi:10.1016/j.cell.2019.09.010 Medline

14. H. Song, E. Yao, C. Lin, R. Gacayan, M.-H. Chen, P.-T. Chuang, Functional characterization of pulmonary neuroendocrine cells in lung development, injury, and tumorigenesis. *Proc. Natl. Acad. Sci. U.S.A.* **109**, 17531–17536 (2012). doi:10.1073/pnas.1207238109 Medline

15. D. T. Montoro, A. L. Haber, M. Biton, V. Vinarsky, B. Lin, S. E. Birket, F. Yuan, S. Chen, H. M. Leung, J. Villoria, N. Rogel, G. Burgin, A. M. Tsankov, A. Waghray, M. Slyper, J.

Waldman, L. Nguyen, D. Dionne, O. Rozenblatt-Rosen, P. R. Tata, H. Mou, M. Shivaraju, H. Bihler, M. Mense, G. J. Tearney, S. M. Rowe, J. F. Engelhardt, A. Regev, J. Rajagopal, A revised airway epithelial hierarchy includes CFTR-expressing ionocytes. *Nature* **560**, 319–324 (2018). doi:10.1038/s41586-018-0393-7 Medline

16. J. K. Watson, S. Rulands, A. C. Wilkinson, A. Wuidart, M. Ousset, A. Van Keymeulen, B. Göttgens, C. Blanpain, B. D. Simons, E. L. Rawlins, Clonal Dynamics Reveal Two Distinct Populations of Basal Cells in Slow-Turnover Airway Epithelium. *Cell Rep.* **12**, 90–101 (2015). doi:10.1016/j.celrep.2015.06.011 Medline

17. I. M. Keith, J. A. Will, Hypoxia and the neonatal rabbit lung: Neuroendocrine cell numbers, 5-HT fluorescence intensity, and the relationship to arterial thickness. *Thorax* **36**, 767–773 (1981). doi:10.1136/thx.36.10.767 Medline

18. N. S. Track, E. Cutz, Bombesin-like immunoreactivity in developing human lung. *Life Sci.* **30**, 1553–1556 (1982). doi:10.1016/0024-3205(82)90243-0 Medline

19. H. Moosavi, P. Smith, D. Heath, The Feyrter cell in hypoxia. *Thorax* **28**, 729–741 (1973). doi:10.1136/thx.28.6.729 Medline

20. J. Pan, T. Bishop, P. J. Ratcliffe, H. Yeger, E. Cutz, Hyperplasia and hypertrophy of pulmonary neuroepithelial bodies, presumed airway hypoxia sensors, in hypoxia-inducible factor prolyl hydroxylase-deficient mice. *Hypoxia (Auckl.)* **4**, 69–80 (2016). Medline

21. J. R. Rock, S. H. Randell, B. L. M. Hogan, Airway basal stem cells: A perspective on their roles in epithelial homeostasis and remodeling. *Dis. Model. Mech.* **3**, 545–556 (2010). doi:10.1242/dmm.006031 Medline

22. P. R. Tata, H. Mou, A. Pardo-Saganta, R. Zhao, M. Prabhu, B. M. Law, V. Vinarsky, J. L. Cho, S. Breton, A. Sahay, B. D. Medoff, J. Rajagopal, Dedifferentiation of committed epithelial cells into stem cells in vivo. *Nature* **503**, 218–223 (2013). doi:10.1038/nature12777 Medline

23. C. Willam, L. G. Nicholls, P. J. Ratcliffe, C. W. Pugh, P. H. Maxwell, The prolyl hydroxylase enzymes that act as oxygen sensors regulating destruction of hypoxia-inducible factor α. *Adv. Enzyme Regul.* **44**, 75–92 (2004). doi:10.1016/j.advenzreg.2003.11.017 Medline

24. K. Wu, K. Zhou, Y. Wang, Y. Zhou, N. Tian, Y. Wu, D. Chen, D. Zhang, X. Wang, H. Xu, X. Zhang, Stabilization of HIF-1α by FG-4592 promotes functional recovery and neural protection in experimental spinal cord injury. *Brain Res.* **1632**, 19–26 (2016). doi:10.1016/j.brainres.2015.12.017 Medline

25. Z.-J. Dai, J. Gao, X.-B. Ma, K. Yan, X.-X. Liu, H.-F. Kang, Z.-Z. Ji, H.-T. Guan, X.-J. Wang, Up-regulation of hypoxia inducible factor-1α by cobalt chloride correlates with proliferation and apoptosis in PC-2 cells. *J. Exp. Clin. Cancer Res.* **31**, 28 (2012). doi:10.1186/1756-9966-31-28 Medline

26. D. R. Springall, G. Collina, G. Barer, A. J. Suggett, D. Bee, J. M. Polak, Increased intracellular levels of calcitonin gene-related peptide-like immunoreactivity in pulmonary endocrine cells of hypoxic rats. *J. Pathol.* **155**, 259–267 (1988). doi:10.1002/path.1711550312 Medline

27. Y. Kawanami, Y. Morimoto, H. Kim, T. Nakamura, K. Machida, T. Kido, E. Asonuma, K. Yatera, C. Yoshii, M. Kido, Calcitonin gene-related peptide stimulates proliferation of alveolar epithelial cells. *Respir. Res.* **10**, 8 (2009). doi:10.1186/1465-9921-10-8 Medline

28. W. Xie, J. T. Fisher, T. J. Lynch, M. Luo, T. I. A. Evans, T. L. Neff, W. Zhou, Y. Zhang, Y. Ou, N. W. Bunnett, A. F. Russo, M. J. Goodheart, K. R. Parekh, X. Liu, J. F. Engelhardt, CGRP induction in cystic fibrosis airways alters the submucosal gland progenitor cell niche in mice. *J. Clin. Invest.* **121**, 3144–3158 (2011). doi:10.1172/JCI41857 Medline

29. H. Doods, G. Hallermayer, D. Wu, M. Entzeroth, K. Rudolf, W. Engel, W. Eberlein, Pharmacological profile of BIBN4096BS, the first selective small molecule CGRP antagonist. *Br. J. Pharmacol.* **129**, 420–423 (2000). doi:10.1038/sj.bjp.0703110 Medline

30. P. Tinits, Oxygen therapy and oxygen toxicity. *Ann. Emerg. Med.* **12**, 321–328 (1983). doi:10.1016/S0196-0644(83)80520-4 Medline

31. S. Caimmi, A. Licari, D. Caimmi, A. Rispoli, E. Baraldi, F. Calabrese, G. L. Marseglia, Neuroendocrine cell hyperplasia of infancy: An unusual cause of hypoxemia in children. *Ital. J. Pediatr.* **42**, 84 (2016). doi:10.1186/s13052-016-0295-y Medline

32. E. R. Spindel, M. E. Sunday, H. Hofler, H. J. Wolfe, J. F. Habener, W. W. Chin, Transient elevation of messenger RNA encoding gastrin-releasing peptide, a putative pulmonary growth factor in human fetal lung. *J. Clin. Invest.* **80**, 1172–1179 (1987). doi:10.1172/JCI113176 Medline

33. J. R. Gosney, Pulmonary neuroendocrine cells in species at high altitude. *Anat. Rec.* **236**, 105–107, discussion 108–112 (1993). doi:10.1002/ar.1092360114 Medline

34. K. Aita, M. Doi, K. Tanno, H. Oikawa, Myo-Thaik-Oo, N. Ohashi, S. Misawa, Pulmonary neuroendocrine cell distribution in sudden infant death syndrome. *Leg. Med.* **2**, 134–142 (2000). doi:10.1016/S1344-6223(00)80013-9 Medline

35. P. M. A. Siren, SIDS-CDF hypothesis revisited: Explaining hypoxia in SIDS. *Ups. J. Med. Sci.* **121**, 199–201 (2016). doi:10.1080/03009734.2016.1176972 Medline

36. J. Battiste, A. W. Helms, E. J. Kim, T. K. Savage, D. C. Lagace, C. D. Mandyam, A. J. Eisch, G. Miyoshi, J. E. Johnson, Ascl1 defines sequentially generated lineage-restricted neuronal and oligodendrocyte precursor cells in the spinal cord. *Development* **134**, 285–293 (2007). doi:10.1242/dev.02727 Medline

37. D.-K. Lee, Y. Liu, L. Liao, F. Wang, J. Xu, The prostate basal cell (BC) heterogeneity and the p63-positive BC differentiation spectrum in mice. *Int. J. Biol. Sci.* **10**, 1007–1017 (2014). doi:10.7150/ijbs.9997 Medline

38. E. L. Rawlins, T. Okubo, Y. Xue, D. M. Brass, R. L. Auten, H. Hasegawa, F. Wang, B. L. M. Hogan, The role of Scgb1a1+ Clara cells in the long-term maintenance and repair of lung airway, but not alveolar, epithelium. *Cell Stem Cell* **4**, 525–534 (2009). doi:10.1016/j.stem.2009.04.002 Medline

39. I. H. Jain, L. Zazzeron, R. Goli, K. Alexa, S. Schatzman-Bone, H. Dhillon, O. Goldberger, J. Peng, O. Shalem, N. E. Sanjana, F. Zhang, W. Goessling, W. M. Zapol, V. K. Mootha, Hypoxia as a therapy for mitochondrial disease. *Science* **352**, 54–61 (2016). doi:10.1126/science.aad9642 Medline

40. H. Mou, V. Vinarsky, P. R. Tata, K. Brazauskas, S. H. Choi, A. K. Crooke, B. Zhang, G. M. Solomon, B. Turner, H. Bihler, J. Harrington, A. Lapey, C. Channick, C. Keyes, A. Freund, S. Artandi, M. Mense, S. Rowe, J. F. Engelhardt, Y.-C. Hsu, J. Rajagopal, Dual SMAD Signaling Inhibition Enables Long-Term Expansion of Diverse Epithelial Basal Cells. *Cell Stem Cell* **19**, 217–231 (2016). doi:10.1016/j.stem.2016.05.012 Medline